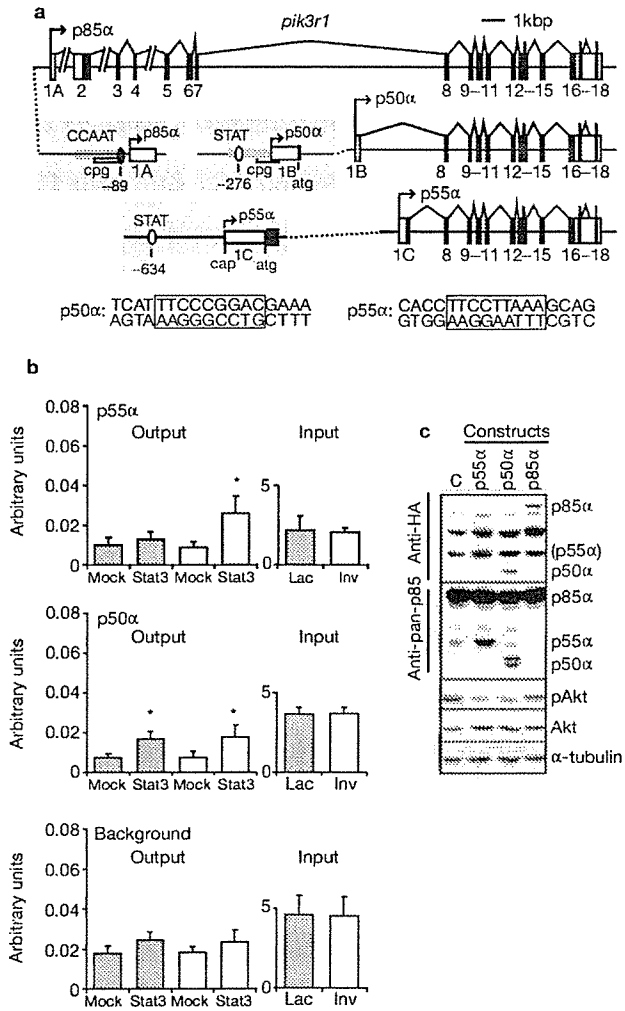

Figure 5 Expression of p55α and p50α is directly regulated by Stat3 *in vivo* and reduces levels of pAkt *in vitro*. (a) Genomic structure of *pik3r1* gene. The mouse *pik3r1* gene contains 20 exons spanning 84.76 kb. Intron 1 spans 9.9 kb and intron 2 47.8 kb. Boxes denote exons and filled boxes denote translated exons. Putative promoter regions are shown in enlarged format. Regions identified using PromoterInspector and FirstEF (p85α and p50α) are shown in grey boxes. The transcription start site for p55α was identified from the 5′ end of oligo-capped mRNA. (b) ChIP assays were performed on glands from lactating (grey) and involuting (white) mice using promoter-specific primers that span the Stat3-binding site and real-time PCR. The assay background was determined using primers directed against an upstream non-promoter sequence. Asterisks denote statistical significance ($^*P<0.05$) in a two-tailed Student's *t*-test comparing isotype-matched control IgG (mock) with Stat3-specific antibody. Graphs show means ± s.d. of lactation (grey) or involution (white) timepoints. (c) Adenovirus-mediated over-expression of the p55α, p50α and p85α regulatory subunits in differentiated KIM-2 cells. Expression of the subunits was assessed by immunoblot with an antibody that recognizes the HA tag (upper panel) and the pan-p85 antibody (middle panel). The p55α is masked by an unspecific band in the HA immunoblot but is clearly visible with the pan-p85 antibody. Decreased levels of pAkt were detected in the extracts from the p55α and p50α over-expressing cells but not in the p85α over-expressing cells (bottom panel), whereas total Akt and α-tubulin levels were unchanged.

evidence that Stat3 binding to the p55α promoter is independent of Stat3 binding to the p50α promoter and is thus indisputably dependent on phosphorylation and activation of Stat3. We conclude that expression of the p85α, p50α and p55α transcripts from the *pik3r1* gene is regulated by distinct, subunit-specific promoters and that expression of p55α and p50α is regulated directly by Stat3.

Our results identify the two PI(3)K regulatory subunits p55α and p50α as direct transcriptional targets of Stat3 *in vivo* and show that upregulation of p55α and p50α is associated with reduced PI(3)K-Akt/PKB signalling. This was confirmed by over-expression of the three *pik3r1* subunits in fully differentiated mammary epithelial cells (Fig. 5c). These results show directly that expression of either p55α or p50α, but not p85α, results in diminished levels of pAkt/PKB. We propose, therefore, the existence of a previously unknown pro-apoptotic pathway by which Stat3 mediates a molecular switch in the subunit composition of PI(3)K, via activation of subunit-specific promoters, to downregulate Akt/PKB survival signalling, and suggest that this is a mechanism by which Stat3 exerts its pro-apoptotic function in mammary epithelial cells. This intriguing result provides an insight into the role of constitutively active Stat3 in carcinogenesis[8] and it will be interesting to determine whether dysregulated Stat3 mediates its oncogeneic effects by failing to induce the switch in PI(3)K subunit composition. Furthermore, in a mouse model of obesity and non-insulin-dependent diabetes mellitus, the *ob/ob* mouse, it has been shown that the levels of p55α and p50α subunits are elevated in liver[26]. Fatty livers from *ob/ob* mice are characterized by hyperactivation of Stat3 (ref. 27), and it is tempting to speculate that these two events are linked.

Taken together, these data strongly suggest that Stat3-mediated regulation of p55α and p50α determines the response of cells to environmental signals through modulating the activity of the PI(3)K-Akt/PKB pathway. □

METHODS

Generation of mice and tissues. The generation and genotyping of conditional Stat3 knockout mice and LIF-deficient mice has been described previously[3,7,28]. Mammary tissue was collected from Stat3$^{-/-}$, Stat3$^{-/+}$, LIF$^{-/-}$ and LIF$^{-/+}$ and wild-type mice after 10 days of lactation and 2 days following forced involution, initiated by removal of the pups after 10 days of lactation. All animals were killed by cervical dislocation. Whole abdominal mammary glands were removed followed by excision of lymph nodes and were snap-frozen in liquid nitrogen for protein or RNA extraction. For sectioning, whole glands were fixed in formalin and embedded in paraffin.

Cell culture and transfection. The mouse mammary epithelial cell line KIM-2 was established and cultured as described previously[7]. The Stat3-GyrB construct subcloned into pMX-puro for retroviral transduction was generated by M. Farrar and kindly provided by A. Mui (University of British Columbia, Canada). The generation of Stat3- and Stat5-GyrB pMX-puro constructs were generated as described[22] and stably introduced into KIM-2 cells. ES cells were cultured as described[23] and the gp130 mutant ES cells were generated as described[23]. KIM-2 cells were treated with LIF (50 ng ml^{-1}) for either 4 or 24 h and cells were collected for immunoblotting as described below.

Adenovirus-mediated expression of PI(3)K regulatory subunits. Adenoviral constructs and supernatants were prepared as described previously[20]. KIM-2 cells were differentiated for 12 days with differentiation media (DMEM/F12 containing 10% FCS and the lactogenic hormones prolactin, dexamethasone and insulin) as previously described[7] and infected with recombinant adenovirus encoding haemagglutinin (HA)-tagged p50α, p55α or p85α subunit sequences in the presence of differentiation media. Cells were collected 18 h post-infection and processed for immunoblotting as described below.

Immunoblotting. Lymph node-free abdominal mammary glands and cells were extracted with a lysis buffer containing 50 mM Tris-HCl pH 7.4, 1% NP-40, 0.25% Na-deoxycholate, 150 mM NaCl, 1 mM EDTA, 1 mM PMSF, 1 μg ml^{-1} aprotinin,

1 μg ml^{-1} leupeptin, 1 μg ml^{-1} pepstatin, 20 μg ml^{-1} bestatin, 20 μM TPCK, 1 mM Na_3VO_4, 1 mM NaF, 5 mM $Na_4P_2O_7$ as described previously[7]. Protein concentration was determined with the BCA colorimetric assay (Pierce, Rockford, IL) and immunoblotting and antibody detection using enhanced chemiluminescence (ECL, Amersham pharmacia biotech, Piscataway, NJ) were performed using standard procedures. The following rabbit antibodies from Cell Signaling Technology (Beverly, MA) were used: anti-pAkt/PKB (Ser473), anti-total Akt/PKB, anti-PTEN, anti-cleaved caspase-3 and anti-phospho-Stat3 (Tyr 701). Other commercial antibodies used were mouse anti-stat3 (Transduction Laboratories, Lexington, KY), rat anti-α-tubulin (Abcam, Cambridge, UK), rabbit anti-HA tag (Santa Cruz Biotechnology, Santa Cruz, CA) and a rabbit anti-pan-p85 (Upstate Biotechnology, Lake Placid, NY). The anti-pan-p85 antibody recognizes the p85α, p55α and p50α isoforms, and cross-reacts weakly with p85β and p55γ (ref. 19; data not shown). The class IA regulatory subunit-specific antibodies were directed against the unique N termini of the p85α, p85β, p55α and p55γ, respectively, as described[13,15]. The p55γ antibody recognizes both p55γ and an additional protein of similar molecular weight (data not shown). The generation of isoform-selective antibodies to p110α, p110β and p110δ have been described previously[29]. Secondary HRP-conjugated antibodies were from Dako Cytomation, Glostrup, Denmark.

PI(3)K assay and immunoprecipitation. Proteins (500 μg) from lymph node-free abdominal mammary glands were immunoprecipitated using pan-p85 antibodies or non-immune control antibodies (rabbit anti-mouse IgG), and immunocomplex kinase assays were performed with PtdIns-4,5-bisphosphate as substrate essentially as described[29]. The phospholipids were resolved by thin-layer chromatography and radioactivity was quantified on Molecular Imager FX (Bio-Rad, Hercules, CA). The number indicate the radioactivity in the PtdIns-3,4,5-trisphosphate spot after subtraction of the radioactivity in a non-immune control precipitate, expressed as arbitrary PhosphorImager units.

Immunofluorescence and TUNEL assay. Immunofluorescene was performed using immunohistochemistry-specific rabbit-anti pAkt/PKB (Ser 473) antibodies (Cell Signaling Technology) and secondary Alexa Flour 488 goat anti-rabbit antibodies (Molecular probes, Eugene, OR) according to the supplier's instructions. TUNEL staining of paraffin-embedded sections was performed using ApopTag (Serological Corporation, Norcross, GA) according to the manufacturer's recommendations. Stained slides were mounted in Vectashield containing DAPI (Vector Labs, Burlingame, NH) and photographed under an inverted epi-fluorescence microscope (Leica, Bannockburn, IL).

RNA analysis. Total RNA was extracted from frozen tissue using the TRIzol reagent (Invitrogen, Paisley, UK) followed by additional column purification (Rneasy; Qiagen GmbH, Hilden, Germany). RNA integrity was monitored with Lab-on-a-chip 2100 Bioanalyzer (Agilent Technologies, Palo Alto, UK). cDNA was synthesized by random hexanucleotide-primed reverse transcription from 1 μg of total RNA using the Transcriptor reverse transcription cDNA synthesis kit (Roche, Basel, Switzerland). Quantitative detection of p85α, p55α, p50α, Socs3, and c-fos cDNA was performed using iCycler supermix (Bio-Rad) with the addition of flourescein and SYBR-green according to the supplier's recommendations. The real-time PCR reactions were run in an iCycler (Bio-Rad, Hercules, CA) in triplicate. The following forward and reverse primer pairs were used for specific amplification: p85α, 5′-GCC CCG TGC TTT TCA GAT TTC-3′, 5′-TCC TGC TGG TAT TTG GAC ACT GGG TAG-3′; p55α, 5′-GTT ACA GTG CGG GCC GTA TAG GTT TTA-3′, 5′-TCC TGC TGG TAT TTG GAC ACT GGG TAG-3′; p50α, 5′-CTG GCA GTT CAA AGC GAA ACC GT-3′, 5′-TCC TGC TGG TAT TTG GAC ACT GGG TAG-3′; SOCS-3, 5′-CCC GCG GGC ACC TTT CTT ATC-3′, 5′-TGC TTC GGG GGT CAC TCT GC-3′; c-fos, 5′-AGC GCA GAG CAT CGG CAG AAG-3′, 5′-GTT GAG AAG GGG CAG GGT GAA GG-3′; and cyclophilin, 5′-GACGCCACTGTCGCTTTTCG-3′, 5′-CTT GCCATCCAGCCATTCAGTC-3′. The expression values obtained were normalized against those obtained from control cyclophilin via a standard curve generated by serial dilution of pooled mammary gland cDNA.

Bioinformatics. The genomic organization of the mouse *pik3r1* gene was identified by mapping mRNA for p85α (GenBank accession number U50413), p55α (GenBank accession number AK046259) and p50α (GenBank accession number U50414) to the genomic sequence of mouse chromosome 13 (GenBank accession number AC107662) using BLAST (http://www.ncbi.nlm.nih.gov/blast/bl2seq/bl2.html) and the GenePalette software. One hundred kilobases (kb) of genomic sequence surrounding the *pik3r* gene were screened for the presence of potential promoter regions using PromoterInspector in the GenomatixSuite (http://www.Genomatix.de). Only sequences 5′-flanking exon 1A (p85α) and exon 1B (p50α) were identified as putative promoters in this region. These findings were confirmed using FirstEF[30]. The sequence encoding *p55α* mRNA (AK046259) was originally obtained by the oligo-capping method and the 5′ end of this sequence thus identifies the location of transcription initiation site and core promoter. CpG islands were identified using FirstEF and transcription factor binding sites by eye and by MatInspector (http://www.Genomatix.de).

Chromatin immunoprecipitation assay. ChIP assays were performed using the ChIP kit from Upstate Biotechnology (Lake Placid, NY) with the following modifications. Mammary glands from 10 day lactating and 2 day involuting mice were collected as described above, snap-frozen and ground into a powder under liquid nitrogen. The tissue was fixed in 1% formaldehyde/PBS supplemented with the Complete protease inhibitor cocktail (Roche Diagnostics, Basel, Switzerland), 1 mM Na_3VO_4 and 1 μg ml^{-1} pepstatin for 15 min at room temperature. Fixation was stopped by the addition of glycine to a final concentration of 125 mM. After several washes in ice-cold PBS, the tissue pellet was resuspended in NEBA buffer (10 mM HEPES, 10 mM KCl, 0.1 mM EDTA, 0.1 mM EGTA) supplemented with Complete protease inhibitor cocktail, 1 mM Na_3VO_4 and 1 μg ml^{-1} pepstatin, dounce homogenized and incubated for 15 min on ice. NP40 (0.5%) was added and samples were vortexed for 30 s before collecting the nuclei. Subsequently, the nuclear fraction was lysed in nuclear lysis buffer (50 mM Tris-HCl pH 8.1, 10 mM EDTA, 1% SDS, Complete protease inhibitor cocktail, 1 mM vanadate and 1 μg ml^{-1} pepstatin). Chromatin was sheared by sonication to a size of approximately 500 base pairs (bp), and samples were precleared for 2 h at 4 °C with salmon-sperm DNA–saturated protein-A/G Sepharose. Chromatin solutions were precipitated overnight at 4 °C with 2 μg of anti-Stat3 antibody (sc-482, Santa Cruz Biotechnology) or 2 μg of isotype-matched control IgG (Dako Cytomation). Immune complexes were collected with salmon-sperm DNA– saturated protein-A/G Sepharose for 3 h and were washed extensively following the manufacturer's protocol. Input and immunoprecipitated chromatin were incubated at 65 °C overnight with 0.3 M NaCl and 30 μg RNAse to reverse crosslinks. After proteinase K digestion, DNA was extracted with phenol and chloroform and was ethanol precipitated with 20 μg glycogen as carrier. Input and bound DNA was detected quantitatively by real-time PCR as described above using specific primers to amplify a 297 bp region (−244 to −541) spanning the Stat-binding site (−276) in the mouse p50α promoter and specific primers to amplify a 260 bp region (−375 to −635) spanning the Stat-binding site (−624) in the mouse p55α promoter. Assay background was determined using primers (−7130 to −7282 from p50α transcription start site) to amplify a product of 146 bp. The sequences of the PCR primers used are as follows: p50α, 5′-GTG GCC GAG GCA AGA CTA AC-3′, 5′-CTG CGG GGC TGA CTG TG-3′; p55α, 5′-ATC AGA TAT CCC AAG GTC AAA ACA AGA-3′, 5′-ACC TTC CTT AAA GCA GCT AGC AAT GAG-3′; background, 5′-GGC CAC TCA TCA GCT CTC ACC CAT AC-3′, 5′-GCT CTC TCA AGC CTC CAG CAA AAA CC-3′. Arbitrary concentrations of the amplified products were determined against a serial dilution of genomic DNA.

BIND identifiers. One BIND identifier (www.bind.ca) is associated with this manuscript: 217739.

Note: Supplementary Information is available on the Nature Cell Biology website.

ACKNOWLEDGEMENTS

This work was supported by BBSRC grant number G18086. A.B. was supported by the Ludwig Institute for Cancer Research and by FIRB 2001 (Italy). We thank P. Came and F. Baxter for providing the TUNEL data, T. Rich and B. Kedjouar for critical reading of the manuscript, D. Vetrie for advice on ChIP assay, and A. Tolkovsky and C. Goemans for help with the adenovirus assays.

COMPETING FINANCIAL INTERESTS

The authors declare that they have no competing financial interests.

Received 25 November 2004; accepted 25 February 2005
Published online at http://www.nature.com/naturecellbiology.

1. Schulze-Bergkamen, H. & Krammer, P. H. Apoptosis in cancer-implications for therapy. *Semin. Oncol.* **31,** 90–119 (2004).
2. Kumar, R., Vadlamudi, R. K. & Adam, L. Apoptosis in mammary gland and cancer. *Endocr. Relat. Cancer* **7,** 257–269 (2000).
3. Chapman, R. S. *et al.* Suppression of epithelial apoptosis and delayed mammary gland involution in mice with a conditional knockout of Stat3. *Genes Dev.* **13,** 2604–2616 (1999).
4. Schwertfeger, K. L., Richert, M. M. & Anderson, S. M. Mammary gland involution is delayed by activated Akt in transgenic mice. *Mol. Endocrinol.* **15,** 867–881 (2001).
5. Franke, T. F. *et al.* The protein kinase encoded by the Akt proto-oncogene is a target of the PDGF-activated phosphatidylinositol 3-kinase. *Cell* **2,** 727–736 (1995).
6. Levy, D. E. & Darnell, J. E. Jr. Stats: transcriptional control and biological impact. *Nature Rev. Mol. Cell Biol.* **3,** 651–662 (2002).
7. Kritikou, E. A. *et al.* A dual, non-redundant, role for LIF as a regulator of development and STAT3-mediated cell death in mammary gland. *Development* **130,** 3459–3468 (2003).
8. Yu, H. & Jove, R. The STATs of cancer - new molecular targets come of age. *Nature Rev. Cancer* **4,** 97–105 (2004).
9. Stambolic, V. *et al.* Negative regulation of PKB/Akt-dependent cell survival by the tumor suppressor PTEN. *Cell* **95,** 29–39 (1998).
10. Otsu, M. *et al.* Characterization of two 85 kd proteins that associate with receptor tyrosine kinases, middle-T/pp60c-src complexes, and PI3-kinase. *Cell* **65,** 91–104 (1991).
11. Pons, S. *et al.* The structure and function of p55PIK reveal a new regulatory subunit for phosphatidylinositol 3-kinase. *Mol. Cell Biol.* **15,** 4453–4465 (1995).
12. Antonetti, D. A., Algenstaedt, P. & Kahn, C. R. Insulin receptor substrate 1 binds two novel splice variants of the regulatory subunit of phosphatidylinositol 3-kinase in muscle and brain. *Mol. Cell Biol.* **16,** 2195–2203 (1996).
13. Inukai, K. *et al.* A novel 55-kDa regulatory subunit for phosphatidylinositol 3-kinase structurally similar to p55PIK is generated by alternative splicing of the p85 gene. *J. Biol. Chem.* **271,** 5317–5320 (1996).
14. Fruman, D. A., Cantley, L. C. & Carpenter, C. L. Structural organization and alternative splicing of the murine phosphoinositide 3-kinase p85 alpha gene. *Genomics* **37,** 113–121 (1996).
15. Inukai, K. *et al.* p85 gene generates three isoforms of regulatory subunit for phosphatidylinositol 3-kinase (PI 3-Kinase), p50, p55, and p85, with different PI 3-kinase activity elevating responses to insulin. *J. Biol. Chem.* **272,** 7873–7882 (1997).
16. Vanhaesebroeck, B., Leevers, S. J., Panayotou, G. & Waterfield, M. D. Phosphoinositide 3-kinases: a conserved family of signal transducers. *Trends Biochem. Sci.* **22,** 267–272 (1997).
17. Cantley, L. C. The phosphoinositide 3-kinase pathway. *Science* **296,** 1655–1657 (2002).
18. Ueki, K., Algenstaedt, P., Mauvais-Jarvis, F. & Kahn, C. R. Positive and negative regulation of phosphoinositide 3-kinase-dependent signaling pathways by three different gene products of the p85 regulatory subunit. *Mol. Cell Biol.* **20,** 8035–8046 (2000).
19. Ueki, K. *et al.* Molecular balance between the regulatory and catalytic subunits of phosphoinositide 3-kinase regulates cell signaling and survival. *Mol. Cell Biol.* **22,** 965–977 (2002).
20. Inukai, K. *et al.* Five isoforms of the phosphatidylinositol 3-kinase regulatory subunit exhibit different associations with receptor tyrosine kinases and their tyrosine phosphorylations. *FEBS Lett.* **490,** 32–38 (2001).
21. O'Farrell, A. M., Liu, Y., Moore, K. W. & Mui, A. L. IL-10 inhibits macrophage activation and proliferation by distinct signaling mechanisms: evidence for Stat3-dependent and -independent pathways. *EMBO J.* **16,** 1006–1018 (1998).
22. Leaman, D. W. *et al.* Roles of JAKs in activation of STATs and stimulation of c-fos gene expression by epidermal growth factor. *Mol. Cell Biol.* **16,** 369–375 (1996).
23. Niwa, H., Burdon, T., Chambers, I. & Smith, A. Self-renewal of pluripotent embryonic stem cells is mediated via activation of STAT3. *Genes Dev.* **12,** 2048–2060 (1998).
24. Burdon, T., Smith, A. & Savatier, P. Signalling, cell cycle and pluripotency in embryonic stem cells. *Trends Cell Biol.* **12,** 432–438 (2002).
25. Hallmann, D. *et al.* Altered signaling and cell cycle regulation in embryonal stem cells with a disruption of the gene for phosphoinositide 3-kinase regulatory subunit p85. *J. Biol. Chem.* **278,** 5099–5108 (2003).
26. Kerouz, N. J., Horsch, D., Pons, S. & Kahn, C. R. Differential regulation of insulin receptor substrates-1 and -2 (IRS-1 and IRS-2) and phosphatidylinositol 3-kinase isoforms in liver and muscle of the obese diabetic (*ob/ob*) mouse. *J. Clin. Invest.* **100,** 3164–3172 (1997).
27. Torbenson, M. *et al.* STAT-3 overexpression and p21 up-regulation accompany impaired regeneration of fatty livers. *Am. J. Pathol.* **161,** 155–161 (2002).
28. Dani, C. *et al.* Paracrine induction of stem cell renewal by LIF-deficient cells: a new ES cell regulatory pathway. *Dev. Biol.* **203,** 149–162 (1998).
29. Vanhaesebroeck, B. *et al.* Distinct PI(3)Ks mediate mitogenic signalling and cell migration in macrophages. *Nature Cell Biol.* **1,** 69–71 (1999).
30. Davuluri, R. V., Grosse, I. & Zhang, M. Q. Computational identification of promoters and first exons in the human genome. *Nature Genet.* **4,** 412–417 (2001). Erratum in *Nature Genet.* **3,** 459 (2002).

Am J Physiol Endocrinol Metab 289: E474–E481, 2005.
First published May 10, 2005; doi:10.1152/ajpendo.00003.2005.

Glycogen debranching enzyme association with β-subunit regulates AMP-activated protein kinase activity

Hideyuki Sakoda,[1] Midori Fujishiro,[1] Junko Fujio,[1] Nobuhiro Shojima,[1] Takehide Ogihara,[2] Akifumi Kushiyama,[1] Yasushi Fukushima,[1] Motonobu Anai,[3] Hiraku Ono,[3] Masatoshi Kikuchi,[3] Nanao Horike,[4] Amelia Y. I. Viana,[4] Yasunobu Uchijima,[4] Hiroki Kurihara,[4] and Tomoichiro Asano[4]

[2]Division of Advanced Therapeutics for Metabolic Diseases, Center for Translational and Advanced Animal Research on Human Diseases, Tohoku University Graduate School of Medicine, Sendai; [1]Department of Internal Medicine, Graduate School of Medicine; [3]Institute for Adult Disease, Asahi Life Foundation; and [4]Department of Physiological Chemistry and Metabolism, Graduate School of Medicine, University of Tokyo, Tokyo, Japan

Submitted 4 January 2005; accepted in final form 28 April 2005

Sakoda, Hideyuki, Midori Fujishiro, Junko Fujio, Nobuhiro Shojima, Takehide Ogihara, Akifumi Kushiyama, Yasushi Fukushima, Motonobu Anai, Hiraku Ono, Masatoshi Kikuchi, Nanao Horike, Amelia Y. I. Viana, Yasunobu Uchijima, Hiroki Kurihara, and Tomoichiro Asano. Glycogen debranching enzyme association with β-subunit regulates AMP-activated protein kinase activity. *Am J Physiol Endocrinol Metab* 289: E474–E481, 2005. First published May 10, 2005; doi:10.1152/ajpendo.00003.2005.—AMP-activated protein kinase (AMPK) regulates both glycogen and lipid metabolism functioning as an intracellular energy sensor. In this study, we identified a 160-kDa protein in mouse skeletal muscle lysate by using a glutathione-*S*-transferase (GST)-AMPK fusion protein pull-down assay. Mass spectrometry and a Mascot search revealed this protein to be a glycogen debranching enzyme (GDE). The association between AMPK and GDE was observed not only in the overexpression system but also endogenously. Next, we showed the β1-subunit of AMPK to be responsible for the association with GDE. Furthermore, experiments using deletion mutants of the β1-subunit of AMPK revealed amino acids 68–123 of the β1-subunit to be sufficient for GDE binding. W100G and K128Q, both β1-subunit mutants, are reportedly incapable of binding to glycogen, but both bound GDE, indicating that the association between AMPK and GDE does not involve glycogen. Rather, the AMPK-GDE association is likely to be direct. Overexpression of amino acids 68–123 of the β1-subunit inhibited the association between endogenous AMPK and GDE. Although GDE activity was unaffected, basal phosphorylation and kinase activity of AMPK, as well as phosphorylation of acetyl-CoA carboxylase, were significantly increased. Thus it is likely that the AMPK-GDE association is a novel mechanism regulating AMPK activity and the resultant fatty acid oxidation and glucose uptake.

glutathione-*S* transferase; pull-down assay; mass spectrometry

AMP-ACTIVATED PROTEIN KINASE (AMPK) acts as an intracellular energy sensor and regulates both glycogen and lipid metabolism (1–3). An increased intracellular AMP-to-ATP ratio leads to a conformational change in AMPK; AMPK is then phosphorylated and activated by LKB1. Activated AMPK reportedly phosphorylates and inactivates acetyl-CoA carboxylase (ACC) and decreases in malonyl-CoA, which increases fatty acid oxidation. 3-Hydroxy-3-methylglutaryl coenzyme A (HMG-CoA) reductase is also downregulated by AMPK, and cholesterol synthesis is thereby decreased. In skeletal muscle, contraction and 5-aminoimidazole-4-carboxamide-1-β-D-ribofuranoside (AICAR) stimulation increase AMPK activity and thereby increase GLUT4 translocation and glucose uptake (4). In addition, expression of GLUT4 protein is increased by continuous AICAR stimulation (5, 6), although events downstream from AMPK involving translocation and gene transcription of GLUT4 have not yet been clarified.

Energy storage in cells depends mainly on glycogen and lipid. Recently, it was reported that a considerable amount of AMPK colocalizes with glycogen particles. This has been attributed to the β-subunit of AMPK that contains a glycogen-binding domain (7–9). Although the physiological significance of this localization of AMPK with glycogen particles remains unclear, glycogen synthase was reported to be phosphorylated and deactivated by AMPK in vitro (10). In the skeletal muscle of AMPKα2 knockout mice, basal glycogen synthase activity is increased, and AICAR treatment fails to deactivate glycogen synthase (11). In addition, it was reported that the activation of AMPKα2 is increasingly suppressed as glycogen levels rise (12). Mutation of the AMPK γ-subunit reportedly increase glycogen content in skeletal muscle and the heart (13, 14). Thus AMPK has a close relationship, not only locationally but also functionally, with glycogen.

In this study, we attempted to identify proteins that bind to AMPK by using a glutathione-*S*-transferase (GST)-AMPK fusion protein pull-down assay, and found GDE to be the AMPK-associated protein. Herein, we show that GDE associates with AMPK and thereby modulates its kinase activity.

MATERIALS AND METHODS

Antibodies. The antibodies against the α- and β-subunits of AMPK and GDE were prepared by immunization of rabbits with a GSTα2 subunit, GSTβ1 subunit, and GDE fusion protein, respectively. These antibodies were then affinity purified as previously described (15). Anti-Flag, anti-hyaluronic acid (HA), and anti-c-myc antibody were purchased from Sigma; anti-AMPKβ, anti-phospho-AMPKα-Thr^{172}, and anti-phospho-ACC-Ser^{79} were purchased from Cell Signaling Technology; and anti-AMPKα1-specific antibody and anti-AMPKα2-specific antibody were purchased from Upstate Biotechnology.

Animals. Six-week-old male C57/BL6 mice and Sprague-Dawley rats were purchased from Tokyo Experimental Animals (Tokyo, Japan) and fed a standard rodent diet. Some mice were starved for

Address for reprint requests and other correspondence: Department of Physiological Chemistry and Metabolism, Graduate School of Medicine, University of Tokyo, 7-3-1 Hongo Bunkyo-ku, Tokyo, Japan (e-mail: asanotky@umin.ac.jp).

The costs of publication of this article were defrayed in part by the payment of page charges. The article must therefore be hereby marked "*advertisement*" in accordance with 18 U.S.C. Section 1734 solely to indicate this fact.

12 h; these mice were then anesthetized with pentobarbital sodium (60 mg/kg body wt inositol 1,4,5-trisphosphate), and lower limb skeletal muscles were dissected out. The study protocol was approved by the Institutional Review Board of the Institute for Adult Disease, Asahi Life Foundation. Animal care was in accordance with the policies of the University of Tokyo at all times.

Cell culture. COS-7 cells and HEK293 cells were maintained in DMEM supplemented with 5% fetal bovine serum under a 5% CO_2 atmosphere at 37°C. Sf9 cells were maintained in Grace's medium supplemented with 5% fetal bovine serum at 27°C.

DNA constructs. cDNAs encoding human GDE and the β1-subunit of human AMPK were produced by PCR with primers corresponding to sequences already reported, using the cDNA library from HEK293 cells. All GDE and AMPKβ1 constructs were designed to contain a Flag or HA tag at the COOH terminus. Human AMPKα1, -α2, -β2, -γ1, and -γ2 cDNAs were kindly provided by Japan Tobacco, Central Pharmaceutical Research Institute (Osaka, Japan). W100G and K128Q, both β1-subunit mutants, were produced by PCR as reported previously (8). Fragments of the NH_2-terminal portion (amino acids 1–67), glycogen binding domain (GBD); (amino acids 68–163), and COOH- terminal portion (amino acids 164–270) of the β1-subunit were amplified by PCR with sense primers attached to the *Bam*HI site and a start codon: 5′-GGA TCC ATG GGC AAT ACC AGC AGT-3′, 5′-GGA TCC ATG GAA GTG AAT GAT AAA GCT-3′, or 5′-GGA TCC ATG GAT GCT TTA ATG GTG GA-3′, respectively, and with antisense primers attached to the HA tag and a stop codon: 5′-TCA AGC GTA GTC TGG GAC GTC GTA TGG GTA CAG ATC ATG CTG CCA GGC-3′, 5′-TCA AGC GTA GTC TGG GAC GTC GTA TGG GTA AAA TAC TTC AAA GTC-3′, or 5′-TCA AGC GTA GTC TGG GAC GTC GTA TGG GTA TAT GGG CTT GTA TAA-3′, respectively. The cDNAs encoding amino acids 68–113, 68–123, 68–133, 68–143, and 68–153 in the GBD of AMPKβ1 were amplified by PCR, with 5′-GGA TCC ATG GAA GTG AAT GAT AAA GCT-3′ as the sense primer and 5′-TCA AAA GTT ATT GTG GCT TCT-3′, 5′-TCA ATG CTC TCC TTC CGG-3′, 5′-TCA CCA CTG ACC ATC CAC-3′, 5′-TCA GGT TAC TAT GGG CTC-3′, and 5′-TCA AAT GAT GTT GTT AAC-3′ as antisense primers, respectively. The cDNA-encoding amino acids 113–163 of AMPKβ1 were amplified by PCR with 5′-GGA TCC ATG GTA GCC ATC CTG GAT CTG-3′ as the sense primer and 5′-TCA GTA AAA TAC TTC AAA GTC-3′ as the antisense primer. PCR products were cloned into a pCR2.1 plasmid vector (Invitrogen, San Diego, CA) and all sequences were confirmed using a CEQ2000 DNA Analysis System (Beckman Coulter).

Generation of recombinant adenovirus and baculovirus. Recombinant adenovirus used to express human GDE was constructed by homologous recombination of the expression cosmid cassettes containing the corresponding cDNAs and the parental virus genome, as described previously (16). The full-length coding regions of AMPKα2, including the GST sequence at the NH_2 terminus, AMPKβ1, AMPKγ2, and GDE in the pBacPAK9 transfer vector (Clontech), and the baculoviruses were prepared according to the manufacturer's instructions. For protein production, Sf9 cells were infected with these baculoviruses and grown for 48 h.

Purification of GST-AMPK fusion protein. GST and the GSTα2 subunit were overexpressed in Sf9 cells using baculoviruses and the cells were lysed with lysis buffer (PBS, 1% Triton X-100, 0.2 mmol/l PMSF). GST and the GSTα2 subunit fusion protein were isolated and purified by affinity chromatography on glutathione-Sepharose 4B (Pharmacia Biotech). The purified GST and GSTα2 subunit fusion protein were incubated with Sf-9 lysates of cells co-overexpressing the β1- and γ2-subunits of AMPK for 1 h and then washed six times with lysis buffer and used for the GST pull-down assay.

GST pull-down assay. Muscles were homogenized with 10 vol/wt homogenizing buffer [20 mmol/l Tris·HCl (pH 7.4), 1% Triton X-100, 0.25% sodium deoxycholate, 0.25 mol/l NaCl] containing 0.2 mmol/l PMSF and 5 μg/ml aprotinin and then centrifuged at 15,000 rpm for 30 min at 4°C. Next, the supernatants were recentrifuged at 100,000 *g* for 1 h. Then, 100 ml of supernatant (2 μg/ml protein concentration) were incubated with 1 ml of glutathione-Sepharose 4B for 1 h at 4°C to remove nonspecifically bound proteins, incubated with purified GST-AMPK fusion protein for 1 h, washed six times with homogenizing buffer, subjected to SDS-PAGE, and then silver stained. As a negative control, GST, preincubated only with Sf9 cells overexpressing the β1- and γ2-subunits, was incubated with tissue lysates from mouse skeletal muscle. GST-AMPK fusion protein not incubated with tissue lysates was also subjected to SDS-PAGE. The band specifically observed as an AMPK-associated protein was analyzed using mass spectrometry and Mascot search by Shimadzu Biotech (Ibaragi, Japan).

Purification of GST fusion protein and pull-down assay. cDNAs encoding full-length AMPKα2, AMPKβ1, and AMPKγ1 and fragments of the β1-subunit of AMPK were subcloned into a pGEX-4T-3 vector (Amersham Biosciences) that was used to transform *Escherichia coli* JM109. Transformed cells were grown to an A_{600} of 0.6 in LB medium supplemented with 0.1 mg/ml ampicillin and stimulated for 3 h with 1.0 mM isopropyl-β-D-1-thiogalactopyranoside. GST fusion proteins were isolated and purified by affinity chromatography on glutathione-Sepharose 4B (17). GDE-overexpressing Sf9 cell lysates were immunoprecipitated with anti-Flag M2-agarose (Sigma), and GDE was purified and eluted from the agarose with 3× Flag peptide (Sigma). Purified GDE was incubated with GST, GST containing full-length AMPKα2, AMPKβ1, or AMPKγ1, or various GST fragments of the β1-subunit of AMPK for 1 h. After six washes with lysis buffer, glutathione-Sepharose 4B beads were boiled in Laemmli buffer, followed by SDS-PAGE and Western blotting.

AMPK assay. After first serum-starving COS-7 cells for 2 h in serum-free DMEM, followed by preincubation for 1 h in Krebs-Ringer-HEPES buffer, the cells were stimulated with a 30-min incubation in Krebs-Ringer-HEPES buffer containing 2 mmol/l AICAR. Next, the COS-7 cells were lysed in *buffer A* and centrifuged. The supernatants were then immunoprecipitated with anti-AMPKα antibodies. AMPK activities in the immunoprecipitants were assayed using SAMS peptide, as described previously (15).

Glycogen debranching enzyme assay. After the serum starvation, preincubation, and AICAR stimulation previously described, COS-7 cells overexpressing GDE were collected with Tris buffer [20 mmol/l Tris·HCl (pH 7.5), 1 mmol/l sodium orthovanadate, 1 mmol/l β-glycerophosphate, and 0.2 mmol/l PMSF] and then sonicated. The sonicated cells were centrifuged at 17,000 *g* for 20 min, and the supernatants were immunoprecipitated with anti-Flag antibody. The immunoprecipitants were washed twice with Tris buffer and twice more with GDE assay buffer [20 mmol/l Tris·HCl (pH 7.5), 50 mmol/l sodium acetate]. Next, the immunoprecipitants were incubated at 37°C for 30 min in the GDE assay buffer containing 15 mmol/l glucosyl-β-cyclodextrin as the substrate (18–20), and GDE activities were determined by measuring the amount of glucose released from glucosyl-β-cyclodextrin, using the glucose oxidase method (GLU CII, Wako).

Immunopreciptation and immunoblotting. The supernatants from skeletal muscle and COS-7 cells, prepared as previously described, were immunoprecipitated with 3 μg/ml antibodies for 2 h. The immunoprecipitants were boiled in Laemmli sample buffer containing 100 mmol/l DTT and then subjected to SDS-PAGE and Western blotting with each antibody, as previously described. (21).

RESULTS

GST pull-down assay using GST-AMPK fusion protein-GST-AMPKα2 subunit fusion protein and the β- and γ-subunits were overexpressed in Sf9 cells using baculovirus. After the GSTα2-subunit had been purified with glutathione-Sepharose 4B, Sf9 cell lysates co-overexpressing the β1- and γ2-subunits of AMPK were added to the GST-α2-subunit bound

to glutathione-Sepharose 4B. Employing this procedure, a trimer consisting of α2-, β1-, and γ2-subunits was produced on glutathione-Sepharose 4B beads, although more than half of the α2-subunit was still not bound to the β1- and γ2-subunits. Next, purified GST-AMPK fusion proteins and GST alone were incubated with lysates from mouse skeletal muscle. GST-AMPK fusion and associated proteins were subjected to SDS-PAGE, followed by silver staining (Fig. 1*A*, *lane 2*). As a negative control, GST alone preincubated with β1- and γ2-subunits was incubated with tissue lysates from mouse skeletal muscle (Fig. 1*A*, *lane 1*). In *lane 3* of Fig. 1*A*, corresponding to the GST-AMPK fusion protein, three subunits and several bands derived from Sf9 cell lysates are apparent. A comparison with *lane 1*, corresponding to the GST-alone protein, revealed the 160-kDa single band in *lane 2* to be a protein binding specifically to AMPK. The 160-kDa band was trypsinized and analyzed using mass spectrometry and Mascot search. With the Mascot search method, protein scores exceeding 67 points are significant ($P < 0.05$). Five proteins had significant scores, and the highest, at 258 points, was rabbit GDE. The protein with the second highest score, 217 points, was rat GDE. Human GDE protein had a score of 174 points, the partial sequences of mouse GDE 94 and 75 points. All proteins with significant Mascot search results were GDEs, which consistently had very high scores. The identification of this 160-kDa protein as a GDE was confirmed with immunoblotting using anti-GDE antibody (data not shown). We thus concluded that the 160-kDa protein was, in fact, mouse GDE.

Subsequently, we examined the in vivo association between AMPKα and GDE. Mouse skeletal muscle lysates were immunoprecipitated with anti-AMPKβ antibody (Cell Signaling) or control IgG, and the immunoprecipitants were subjected to SDS-PAGE and immunoblotting using anti-GDE antibody. As shown in Fig. 1*B*, GDE was detected in the AMPKβ immunoprecipitant but not in the control IgG precipitant, which indicates a physiological association between AMPK and GDE. In addition, this association did not differ significantly, depending on whether the mice were fasted or fed.

GDE bound to the AMPKβ1-subunit directly. AMPK consists of a catalytic α-subunit and regulatory β- and γ-subunits. To examine which subunit binds GDE, each subunit and GDE were co-overexpressed in COS-7 cells and immunoprecipitated with each of the anti-tag antibodies. The α1-, α2-, β1-, and β2-subunits of AMPK were coimmunoprecipitated with GDE, whereas the γ1- and γ2-subunits were not (Fig. 2, *A*, *B*, and *C*). The 312 NH_2-terminal amino acid portion of the α-subunit does not bind to the β- and γ-subunits, since the association with the β-subunit is via the COOH-terminal portion of the α-subunit. The 312 NH_2-terminal amino acids of the α-subunit were found to not coimmunoprecipitate with GDE (Fig. 2*A*, *lower middle*). This raised the possibility that the coimmunoprecipitation of the α-subunit with GDE did not represent a direct association but rather binding with the β- or γ-subunit of AMPK.

To confirm that the β- but not the γ-subunit binds to GDE, GDE alone or GDE plus the β1-, β2-, γ1-, or γ2-subunit was overexpressed in COS-7 cells. In the GDE immunoprecipitant, the β1- and β2- but not the γ1- and γ2-subunits were detected (Fig. 2, *B* and *C*, *lower middle*). Similarly, GDE was detected

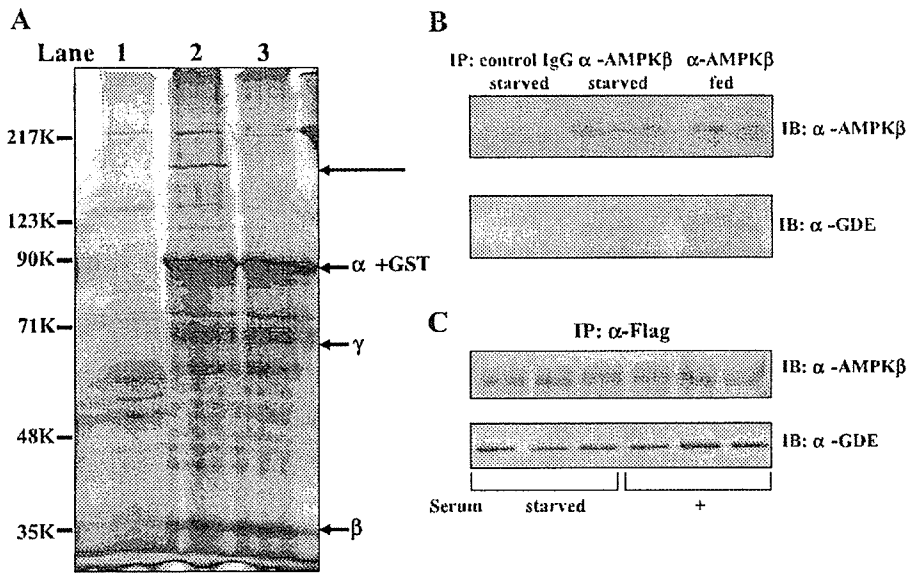

Fig. 1. Pull-down assays using glutathione-*S*-transferase-AMP-activated protein kinase (GST-AMPK) fusion proteins. *A*: GST and GST-AMPKα2 fusion proteins were overexpressed in Sf9 cells by using a baculovirus and then purified with glutathione-Sepharose 4B. Purified GST alone and GST-AMPKα2 fusion proteins were incubated with Sf9 cell lysates overexpressing AMPKβ1 and AMPKγ2 and then with a tissue lysate from mouse skeletal muscle for 1 h. Beads were washed 6 times with homogenizing buffer followed by SDS-PAGE and silver staining. *Lane 1*: GST alone was incubated with AMPKβ1 and AMPKγ2 and then with lysates from mouse skeletal muscle. *Lane 2*: GST-AMPKα2 was incubated with AMPKβ1 and AMPKγ2 and then with lysates from mouse skeletal muscle. *Lane 3*: GST-AMPKα2 was incubated with AMPKβ1 and AMPKγ2 but not with the mouse skeletal muscle lysate. A 160-kDa band (arrow, *lane 2*) was identified as glycogen debranching enzyme (GDE) by mass spectrometry and Mascot search technique. *B*: lysates from mouse skeletal muscle were immunoprecipitated (IP) with control IgG or anti-AMPKβ antibodies, followed by SDS-PAGE and Western blotting with anti-AMPKβ (*top*) or anti-GDE (*bottom*) antibodies. *C*: Flag-tagged GDE was overexpressed in COS-7 cells with adenoviruses. After being serum starved or not for 12 h, cells were lysed and immunoprecipitated with anti-Flag antibody. Immunoprecipitants were subjected to SDS-PAGE and Western blotting using anti-AMPKβ (*top*), and anti-GDE (*bottom*) antibodies.

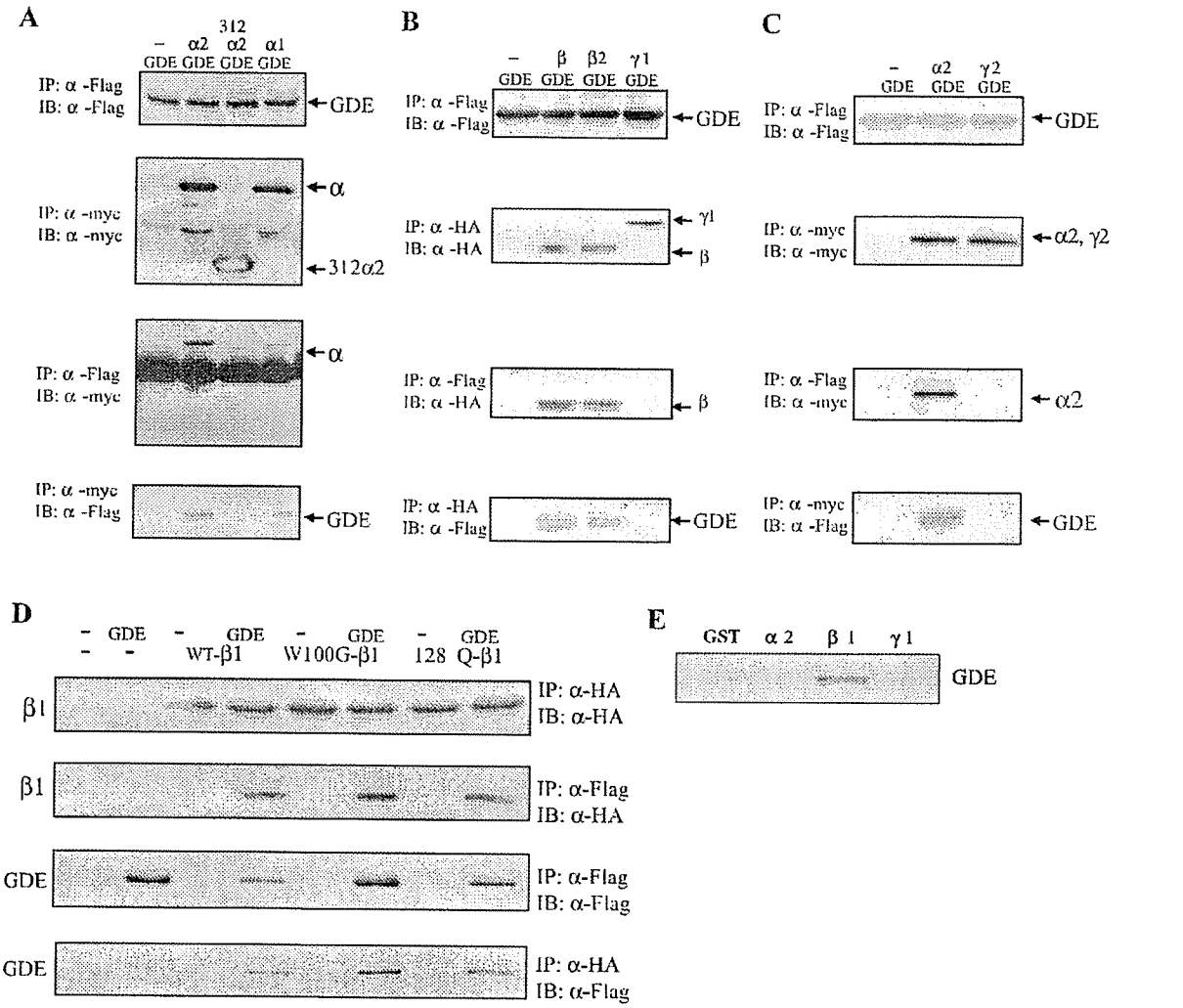

Fig. 2. β-Subunit of AMPK binds to GDE. *A*: GDE (Flag-tagged) and AMPKα2, 312 NH_2-terminal amino acids of AMPKα2, and -α1 (myc-tagged) were co-overexpressed in COS-7 cells. Cell lysates were immunoprecipitated with anti-myc or anti-Flag antibodies followed by SDS-PAGE and Western blotting (IB) with anti-myc or anti-Flag antibodies. *B*: GDE (Flag-tagged) and AMPKβ1, -β2 [(HA)-tagged], and AMPKγ1 (HA-tagged) were co-overexpressed in COS-7 cells. Cell lysates were immunoprecipitated with anti-HA or anti-Flag antibodies followed by SDS-PAGE and Western blotting with anti-HA or anti-Flag antibodies. *C*: GDE (Flag-tagged) and AMPKα2, and -γ2 (myc-tagged) were co-overexpressed in COS-7 cells. Cell lysates were immunoprecipitated with anti-myc or anti-Flag antibodies followed by SDS-PAGE and Western blotting with anti-myc or anti-Flag antibodies, respectively. *D*: GDE (Flag-tagged) and wild-type, W100G, and K128Q AMPKβ1 (HA-tagged) were overexpressed in Sf9 cells by baculoviruses. Cell lysates were immunoprecipitated with anti-HA or anti-Flag antibodies followed by SDS-PAGE and Western blotting with anti-HA or anti-Flag antibodies. *E*: GST fusion proteins containing full-length AMPKα2, -β1, or -γ1 were purified using glutathione-Sepharose 4B, as described in MATERIALS AND METHODS. GDE was purified using anti-FLAG M2-agarose (Sigma) and 3× Flag peptide (Sigma). Purified GDEs were incubated with GST, GST-AMPKα2, GST-AMPKβ1, or GST-AMPKγ1 for 1 h. After 6 washes with lysis buffer, glutathione-Sepharose 4B beads were boiled in Laemmli buffer followed by SDS-PAGE and Western blotting using anti-Flag antibody.

in the β1- and β2- but not the γ1- and γ2-subunit immunoprecipitants (Fig. 2, *B* and *C*, *bottom*).

In addition, pull-down assays were performed using GST-AMPK fusion protein with purified GDE. As shown in Fig. 2*E*, GDEs were pulled down by purified GST-AMPKβ1 fusion protein.

Thus we concluded that the β-subunit is responsible for the association of AMPK with GDE.

Recently, AMPKβ1 was reported to possess a glycogen binding domain (8, 9). GDE also binds to glycogen, and thus we speculate that AMPKβ1 and GDE coimmunoprecipitate through their glycogen binding domains rather than associating directly. To examine this possibility, β1-subunit mutants W100G and K128Q, both of which are incapable of binding glycogen (8), were overexpressed with or without GDE, as well as the wild-type β1-subunit (Fig. 2*D*). It was clearly demonstrated that these glycogen-binding, defective β1-subunit mutants still coimmunoprecipitate with GDE, just like the wild-type β1-subunit. This indicates that the association between the β-subunit and GDE does not involve glycogen but rather is direct.

GDE binding to an AMPK site. To identify the GDE binding site in the β1-subunit, we prepared various deletion mutants of the β1-subunit as GST fusion proteins (Fig. 3*A*). By use of these GST-AMPKβ1 fragment fusion proteins, pull-down assays were performed.

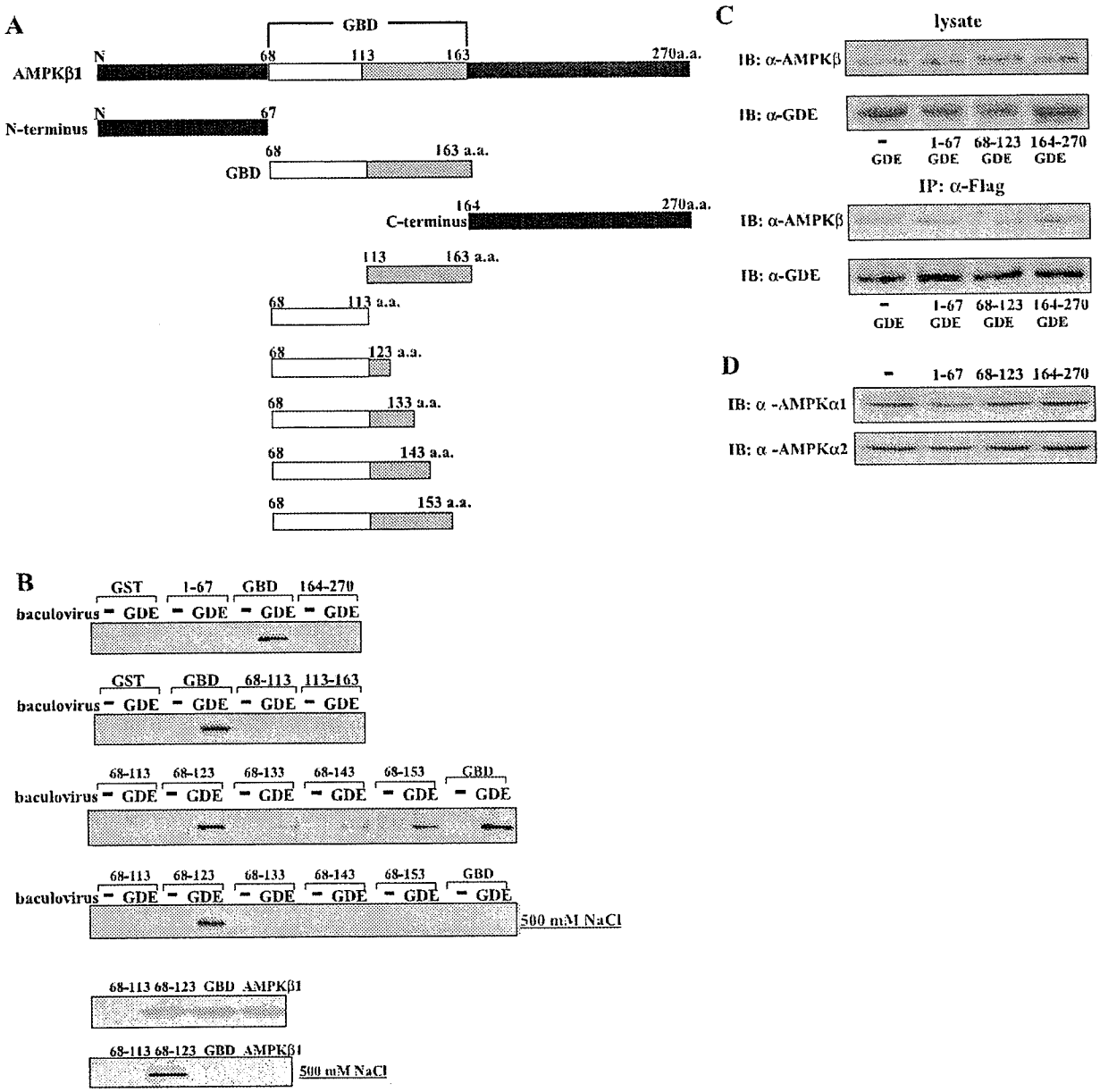

Fig. 3. Amino acids 68–123 of AMPKβ1 include the GDE binding site. *A*: schematic presentation of GST fragment of AMPKβ1 fusion protein. *B*: GST-AMPKβ1 fragment fusion proteins were overexpressed in JM109 and purified with glutathione-Sepharose 4B. Purified GST-AMPK fusion proteins were incubated with GDE (Flag-tagged) overexpressing Sf9 cell lysates for 1 h and then washed 6 times with lysis buffer followed by SDS-PAGE and Western blotting with anti-Flag antibody. The amino acids 68–123 sequence of the β1-subunit bound GDE most strongly. *C* and *D*: GDE and amino acids 1–67, 68–123, or 164–270 of the β1-subunit were overexpressed in COS-7 cells with adenoviruses. *C*: cells were lysed and immunoprecipitated with anti-Flag antibody. Immunoprecipitants were subjected to SDS-PAGE and Western blotting using anti-AMPKβ and anti-GDE antibodies. *D*: overexpression of amino acids 68–123 of the β1-subunit inhibited association of AMPKβ with GDE. Total cell lysates were subjected to SDS-PAGE and Western blotting using anti-AMPKα1- or -α2-specific antibody.

First, GST protein containing three fragments corresponding to the NH_2 terminus, GBD, and COOH terminus of the β1-subunit were purified with glutathione-Sepharose 4B, and the association with GDE was assessed by incubation with the lysate from GDE overexpressing Sf9 cells. Figure 3*B*, *panel 1*, shows clearly that the sequence responsible for the association with GDE is included in the GBD of the β1-subunit (Fig. 3*B*, *panel 1*). Next, GBD was separated into two fragments: amino acids 68–113 and amino acids 113–163 of the β1-subunit. However, we found that these fragments did not bind GDE (Fig. 3*B*, *panel 2*). Thus we prepared four additional β1-subunit deletion mutants of GBD: amino acids 68–123, 68–133, 68–143, and 68–153. Amino acids 68–123, but not 68–113, were demonstrated to be sufficient for binding with GDE (Fig. 3*B*, *panel 3*). Amino acid sequences 68–133 and 68–143 exhibited weaker binding with GDE than amino acids

68–123, although the reason for this is unclear. The binding of amino acids 68–123 with GDE was not abolished by washing with high-salt buffer (containing 500 mM NaCl), whereas those with full-length GBD and amino acid sequences 68–133, 68–143, or 68–153 were apparently reduced (Fig. 3*B*, *panel 4*). Thus it is likely that amino acids 68–123 of the β1-subunit possess a high affinity for GDE.

Inhibition of the association between GDE and AMPK increases AMPK activity. Amino acids 68–123 were used to inhibit the association between AMPK and GDE. Full-length GDE and amino acids 68–123 of the β1-subunit were overexpressed, and GDE was immunoprecipitated with anti-Flag antibody. As shown in Fig. 3*C*, overexpression of amino acids 68–123 of the β1-subunit inhibited the association between GDE and AMPKβ1, whereas the AMPKα1 and α2 protein expression levels were unchanged (Fig. 3*D*).

Under these conditions, we examined GDE or AMPK activities in COS-7 cells. Overexpressing amino acids 68–123 of the β1-subunit did not change GDE activities (Fig. 4*A*). On the other hand, basal AMPK activity increased significantly, by ~30%, compared with control cells (Fig. 4*B*). Basal phosphorylation of AMPKα-Thr^{172} was also increased by 35% (Fig. 4*C*). Phosphorylation of ACC-Ser^{79}, which is reportedly phosphorylated by AMPK, was also approximately doubled when amino acids 68–123 of the β1-subunit were overexpressed without AICAR stimulation (Fig. 4*D*). Thus it is very likely that inhibition of the association between GDE and AMPK increases AMPK activity.

DISCUSSION

AMPK is a regulator of the key enzymes involved in glucose and lipid metabolism, functioning as a fuel gauge sensor. ACC and HMG-CoA reductase are well known to be substrates of AMPK; however, downstream from AMPK, their roles in glucose uptake and glycogen metabolism remain unclear. In this study, we identified GDE as an AMPK-binding protein by using a GST-AMPK pull-down assay. Coimmunoprecipitation of AMPK with GDE was observed not only in overexpression experiments but also endogenously (Fig. 1*B*). In addition, the β-subunit was demonstrated to be responsible for the association with GDE. Interestingly, the portion of the β-subunit that binds with GDE (amino acids 68–123 of AMPKβ1) is included in the sequence that reportedly associates with glycogen (amino acids 68–163 of AMPKβ1). Thus we suspected that the association between the β-subunit and GDE occurs via the binding of glycogen to both the β-subunit and GDE. However, W100G and K128Q, glycogen nonbinding mutants of the β1-subunit, fully retained the ability to bind with GDE, suggesting that the association between the β-subunit and GDE does not involve glycogen binding. Furthermore, we found that adding glycogen to the buffer did not alter the in vitro association between the β-subunit and GDE (data not shown). Taking these two observations into consideration, it is reasonable to assume that the association of the β-subunit of AMPK with GDE is direct.

GDE, a 160-kDa monomeric protein, is widely distributed in bacteria, yeasts, plants, and animals. GDE contains two independent catalytic activities, transferase and glucosidase (22, 23), that are responsible for glycogen degradation. Although glycogen phosphorylase degrades glycogen from its nonreducing ends, leaving dextrin with shortened chains, GDE transfers maltosyl units from the shortened chain to another chain employing its transferase activity. GDE then removes the glycosyl stub using its glucosidase activity. Genetic deficiency

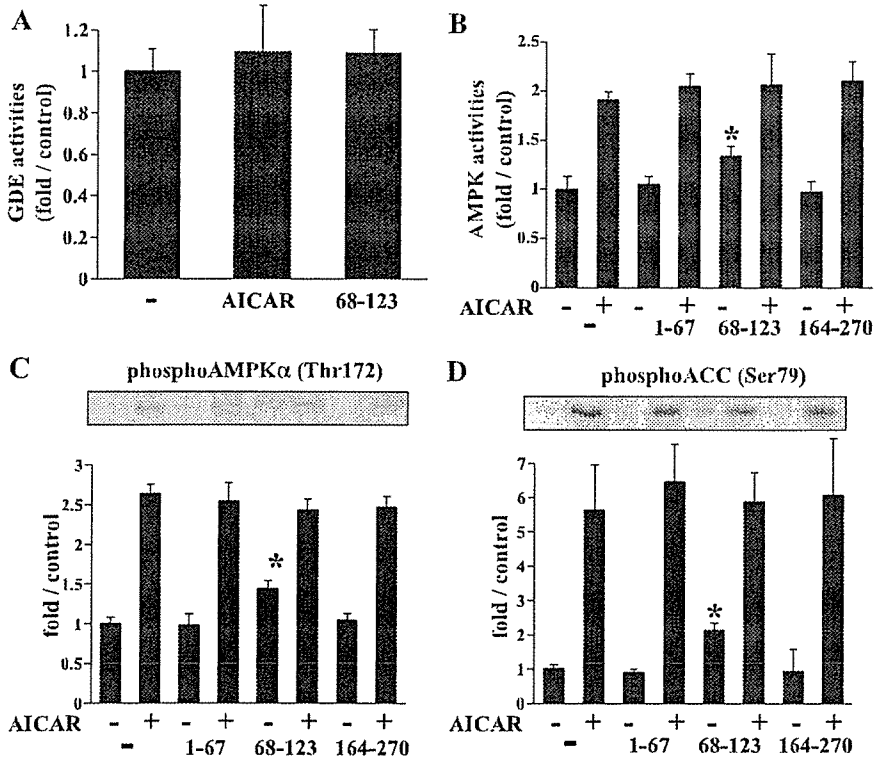

Fig. 4. Inhibition of association between AMPK and GDE increases basal phosphorylation of AMPKα and acetyl-CoA carboxylase (ACC) and also increases basal AMPK activity. *A*: after serum starvation, preincubation, and 5-aminoimidazole-4-carboxamide-1-β-d-ribofuranoside (AICAR) stimulation, as described in RESULTS, GDE-overexpressing COS-7 cells were collected with Tris buffer and then sonicated. Sonicated cells were centrifuged at 17,000 *g* for 20 min, and supernatants were immunoprecipitated with anti-Flag antibody. GDE activities in immunoprecipitants were assayed using glucosyl-β-cyclodextrin as substrate, as described in MATERIALS AND METHODS. Bars depict means ± SE of 3 independent experiments. *B*: COS-7 cells overexpressing amino acids 1–67, 68–123, or 164–270 of the β1-subunit were treated with or without 2 mmol/l AICAR for 30 min. Cells were then lysed and immunoprecipitated with anti-AMPKα antibody. AMPK activities in immunoprecipitants were assayed using SAMS peptide. Bars depict means ± SE of 3 independent experiments. *C* and *D*: COS-7 cells overexpressing amino acids 1–67, 68–123, or 164–270 of the β1-subunit were incubated with or without 2 mmol/l AICAR for 30 min. Cells were then lysed followed by SDS-PAGE and Western blotting using anti-phospho-AMPKα-Thr^{172} (*C*), and anti-phospho-ACC-Ser^{79} (*D*). *$P < 0.05$ vs. control cells (basal).

of GDE in humans is known to cause a type III glycogen storage disorder called Cori's disease (24), which is characterized by hepatomegaly, hypoglycemia, short stature, and muscle weakness (25–27).

A considerable portion of AMPK reportedly colocalizes with glycogen particles, although the physiological significance of this subcellular localization remains unclear. Our results suggest that this subcellular localization of AMPK may be due to binding to GDE but not glycogen or to binding both GDE and glycogen. In addition, we demonstrated herein that amino acids 68–123 of the β1-subunit contain the GDE binding domain. We also showed that overexpression of amino acids 68–123 of the β1-subunit effectively interrupts the binding of endogenous AMPK with GDE and significantly enhances AMPK activity. Thus it is very likely that the association with GDE suppresses the basal kinase activity of AMPK, although how release of the β-subunit from GDE affects the kinase activity of the α-subunit of AMPK remains unknown. We speculate that a decrease in glycogen content may induce dissociation of AMPK from GDE, thereby increasing AMPK activity, which leads to various metabolic actions, including increased glucose uptake and fatty acid oxidation. However, we did not examine the relationship between cellular glycogen contents and the association between AMPK and GDE herein. It is reasonable that upregulating AMPK activity would increase glucose uptake and fatty acid oxidation when cellular glycogen is in short supply. This hypothesis appears to be supported by a previous study showing AMPK activity to be higher in skeletal muscle containing less glycogen (12).

We also speculate that the localization of AMPK is important for its regulation of kinase activity. Many proteins, including protein phosphatase, bind to glycogen, and this binding determines their cellular localizations (8, 9). Furthermore, dissociation from glycogen may change certain protein interactions. AMPK is reportedly activated via phosphorylation of its α-subunit in response to ATP depletion, which is caused by muscle contraction, metabolic poisoning, oxidatative stress, hypoxia, and nutrient deprivation. Increased cellular AMP changes the conformation of the AMPKαβγ complex, revealing the Thr^{172} of the α-subunit to be phosphorylated by LKB-1 (28–30). Thus it is reasonable to speculate that the conformational change in AMPK induced by GDE binding affects the association of AMPK with LKB-1 or some other phosphatase(s). Unfortunately, however, we detected no significant change in the association between AMPK and GDE in response to either fasting or feeding of the mice or with serum starvation of COS-7 cells. Thus although this is the first study to demonstrate a direct association between AMPK and GDE, further studies are needed to clarify how this association is regulated. In addition, it is also necessary to elucidate the resultant physiological significance of this association, which may occur via the regulation of AMPK activity or subcellular localization.

GRANTS

This work was supported by a Grant-in-Aid for Suzuken Memorial foundation (04-042).

REFERENCES

1. **Hardie DG.** Minireview. The AMP-activated protein kinase cascade: the key sensor of cellular energy status. *Endocrinology* 144: 5179–5183, 2003.
2. **Carling D.** The AMP-activated protein kinase cascade–a unifying system for energy control. *Trends Biochem Sci* 29: 18–24, 2004.
3. **Rutter GA, Da Silva Xavier G, and Leclerc I.** Roles of 5'-AMP-activated protein kinase (AMPK) in mammalian glucose homoeostasis. *Biochem J* 375: 1–16, 2003.
4. **Musi N and Goodyear LJ.** AMP-activated protein kinase and muscle glucose uptake. *Acta Physiol Scand* 178: 337–345, 2003.
5. **MacLean PS, Zheng D, Jones JP, Olson AL, and Dohm GL.** Exercise-induced transcription of the muscle glucose transporter (GLUT 4) gene. *Biochem Biophys Res Commun* 292: 409–414, 2002.
6. **Buhl ES, Jessen N, Pold R, Ledet T, Flyvbjerg A, Pedersen SB, Pedersen O, Schmitz O, and Lund S.** Long-term AICAR administration reduces metabolic disturbances and lowers blood pressure in rats displaying features of the insulin resistance syndrome. *Diabetes* 51: 2199–2206, 2002.
7. **Wiatrowski HA, Van Denderen BJ, Berkey CD, Kemp BE, Stapleton D, and Carlson M.** Mutations in the gal83 glycogen-binding domain activate the snf1/gal83 kinase pathway by a glycogen-independent mechanism. *Mol Cell Biol* 24: 352–361, 2004.
8. **Polekhina G, Gupta A, Michell BJ, van Denderen B, Murthy S, Feil SC, Jennings IG, Campbell DJ, Witters LA, Parker MW, Kemp BE, and Stapleton D.** AMPK beta subunit targets metabolic stress sensing to glycogen. *Curr Biol* 13: 867–871, 2003.
9. **Hudson ER, Pan DA, James J, Lucocq JM, Hawley SA, Green KA, Baba O, Terashima T, and Hardie DG.** A novel domain in AMP-activated protein kinase causes glycogen storage bodies similar to those seen in hereditary cardiac arrhythmias. *Curr Biol* 13: 861–866, 2003.
10. **Halse R, Fryer LG, McCormack JG, Carling D, and Yeaman SJ.** Regulation of glycogen synthase by glucose and glycogen: a possible role for AMP-activated protein kinase. *Diabetes* 52: 9–15, 2003.
11. **Wojtaszewski JF, Nielsen JN, Jorgensen SB, Frosig C, Birk JB, and Richter EA.** Transgenic models—a scientific tool to understand exercise-induced metabolism: the regulatory role of AMPK (5'-AMP-activated protein kinase) in glucose transport and glycogen synthase activity in skeletal muscle. *Biochem Soc Trans* 31: 1290–1294, 2003.
12. **Wojtaszewski JF, Jorgensen SB, Hellsten Y, Hardie DG, and Richter EA.** Glycogen-dependent effects of 5-aminoimidazole-4-carboxamide (AICA)-riboside on AMP-activated protein kinase and glycogen synthase activities in rat skeletal muscle. *Diabetes* 51: 284–292, 2002.
13. **Milan D, Jeon JT, Looft C, Amarger V, Robic A, Thelander M, Rogel-Gaillard C, Paul S, Iannuccelli N, Rask L, Ronne H, Lundstrom K, Reinsch N, Gellin J, Kalm E, Roy PL, Chardon P, and Andersson L.** A mutation in PRKAG3 associated with excess glycogen content in pig skeletal muscle. *Science* 288: 1248–1251, 2000.
14. **Gollob MH.** Glycogen storage disease as a unifying mechanism of disease in the PRKAG2 cardiac syndrome. *Biochem Soc Trans* 31: 228–231, 2003.
15. **Sakoda H, Ogihara T, Anai M, Fujishiro M, Ono H, Onishi Y, Katagiri H, Abe M, Fukushima Y, Shojima N, Inukai K, Kikuchi M, Oka Y, and Asano T.** Activation of AMPK is essential for AICAR-induced glucose uptake by skeletal muscle but not adipocytes. *Am J Physiol Endocrinol Metab* 282: E1239–E1244, 2002.
16. **Sakoda H, Gotoh Y, Katagiri H, Kurokawa M, Ono H, Onishi Y, Anai M, Ogihara T, Fujishiro M, Fukushima Y, Abe M, Shojima N, Kikuchi M, Oka Y, Hirai H, and Asano T.** Differing roles of Akt and serum- and glucocorticoid-regulated kinase in glucose metabolism, DNA synthesis, and oncogenic activity. *J Biol Chem* 278: 25802–25807, 2003.
17. **Ogihara T, Isobe T, Ichimura T, Taoka M, Funaki M, Sakoda H, Onishi Y, Inukai K, Anai M, Fukushima Y, Kikuchi M, Yazaki Y, Oka Y, and Asano T.** 14-3-3 Protein binds to insulin receptor substrate-1, one of the binding sites of which is in the phosphotyrosine binding domain. *J Biol Chem* 272: 25267–25274, 1997.
18. **Liu W, de Castro ML, Takrama J, Bilous PT, Vinayagamoorthy T, Madsen NB, and Bleackley RC.** Molecular cloning, sequencing, and analysis of the cDNA for rabbit muscle glycogen debranching enzyme. *Arch Biochem Biophys* 306: 232–239, 1993.
19. **Nakayama A, Yamamoto K, and Tabata S.** Identification *of* the catalytic residues of bifunctional glycogen debranching enzyme, *J Biol Chem* 276: 28824–28828, 2001.
20. **Yanase M, Takata H, Takaha T, Kuriki T, Smith SM, and Okada S.** Cyclization reaction catalyzed by glycogen debranching enzyme (EC 2.4.1.25/EC 3.2.1.33) and its potential for cycloamylose production. *Appl Environ Microbiol* 68: 4233–4239, 2002.

21. **Sakoda H, Ogihara T, Anai M, Funaki M, Inukai K, Katagiri H, Fukushima Y, Onishi Y, Ono H, Yazaki Y, Kikuchi M, Oka Y, and Asano T.** No correlation of plasma cell 1 overexpression with insulin resistance in diabetic rats and 3T3-L1 adipocytes. *Diabetes* 48: 1365–1371, 1999.
22. **Liu W, Madsen NB, Braun C, and Withers SG.** Reassessment of the catalytic mechanism of glycogen debranching enzyme. *Biochemistry* 30: 1419–1424, 1991.
23. **Yang BZ, Ding JH, Enghild JJ, Bao Y, and Chen YT.** Molecular cloning and nucleotide sequence of cDNA encoding human muscle glycogen debranching enzyme. *J Biol Chem* 267: 9294–9299, 1992.
24. **Shen J, Bao Y, Liu HM, Lee P, Leonard JV, and Chen YT.** Mutations in exon 3 of the glycogen debranching enzyme gene are associated with glycogen storage disease type III that is differentially expressed in liver and muscle. *J Clin Invest* 98: 352–357, 1996.
25. **Chen YT, Bali D, and Sullivan J.** Prenatal diagnosis in glycogen storage diseases. *Prenat Diagn* 22: 357–359, 2002.
26. **Shen JJ and Chen YT.** Molecular characterization of glycogen storage disease type III. *Curr Mol Med* 2: 167–175, 2002.
27. **Wolfsdorf JI, Holm IA, and Weinstein DA.** Glycogen storage diseases. Phenotypic, genetic, and biochemical characteristics, and therapy. *Endocrinol Metab Clin North Am* 28: 801–823, 1999.
28. **Woods A, Johnstone SR, Dickerson K, Leiper FC, Fryer LG, Neumann D, Schlattner U, Wallimann T, Carlson M, and Carling D.** LKB1 is the upstream kinase in the AMP-activated protein kinase cascade. *Curr Biol* 13: 2004–2008, 2003.
29. **Hawley SA, Boudeau J, Reid JL, Mustard KJ, Udd L, Makela TP, Alessi DR, and Hardie DG.**Complexes between the LKB1 tumor suppressor, STRAD alpha/beta and MO25 alpha/beta are upstream kinases in the AMP-activated protein kinase cascade. *J Biol* 2, 28: 2003.
30. **Shaw RJ, Kosmatka M, Bardeesy N, Hurley RL, Witters LA, DePinho RA, and Cantley LC.** The tumor suppressor LKB1 kinase directly activates AMP-activated kinase and regulates apoptosis in response to energy stress. *Proc Natl Acad Sci USA* 101: 3329–3335, 2004.

Adenosine Monophosphate-Activated Protein Kinase Suppresses Vascular Smooth Muscle Cell Proliferation Through the Inhibition of Cell Cycle Progression

Motoyuki Igata,* Hiroyuki Motoshima,* Kaku Tsuruzoe, Kanou Kojima, Takeshi Matsumura, Tatsuya Kondo, Tetsuya Taguchi, Kazuhiko Nakamaru, Miyuki Yano, Daisuke Kukidome, Kazuya Matsumoto, Tetsushi Toyonaga, Tomoichiro Asano, Takeshi Nishikawa, Eiichi Araki

Abstract—Vascular smooth muscle cell (VSMC) proliferation is a critical event in the development and progression of vascular diseases, including atherosclerosis. We investigated whether the activation of adenosine monophosphate-activated protein kinase (AMPK) could suppress VSMC proliferation and inhibit cell cycle progression. Treatment of human aortic smooth muscle cells (HASMCs) or isolated rabbit aortas with the AMPK activator 5-Aminoimidazole-4-carboxamide ribonucleoside (AICAR) induced phosphorylation of AMPK and acetyl Co-A carboxylase. AICAR significantly inhibited HASMC proliferation induced by both platelet-derived growth factor-BB (PDGF-BB) and fetal calf serum (FCS). Treatment with AICAR inhibited the phosphorylation of retinoblastoma gene product (Rb) induced by PDGF-BB or FCS, and increased the expression of cyclin-dependent kinase inhibitor $p21^{CIP}$ but not that of $p27^{KIP}$. Pharmacological inhibition of AMPK or overexpression of dominant negative-AMPK inhibited both the suppressive effect of AICAR on cell proliferation and the phosphorylation of Rb, suggesting that the effect of AICAR is mediated through the activation of AMPK. Cell cycle analysis in HASMCs showed that AICAR significantly increased cell population in G0/G1-phase and reduced that in S- and G2/M-phase, suggesting AICAR induced cell cycle arrest. AICAR increased both p53 protein and Ser-15 phosphorylated p53 in HASMCs, which were blocked by inhibition of AMPK. In isolated rabbit aortas, AICAR also increased Ser-15 phosphorylation and protein expression of p53 and inhibited Rb phosphorylation induced by FCS. These data suggest for the first time that AMPK suppresses VSMC proliferation via cell cycle regulation by p53 upregulation. Therefore, AMPK activation in VSMCs may be a therapoietic target for the prevention of vascular diseases. (*Circ Res.* 2005;97:837-844.)

Key Words: AMP-activated protein kinase ■ cell cycle arrest ■ p53 ■ p21 ■ AICAR

Vascular smooth muscle cell (VSMC) proliferation is one of the critical events in the development and progression of various vascular diseases, including atherosclerosis and restenosis after coronary intervention.[1] Mammalian cell proliferation is governed by the cell cycle.[2] Cell cycle progression is a tightly controlled event regulated positively by cyclin-dependent kinases (CDKs) and their cyclin-regulatory subunits,[3] and negatively by CDK inhibitors (CDKIs) and tumor suppressor genes.[4] Mitogenic factors bind to their receptors and initiate a series of events resulting in the activation of CDKs, which in turn regulates cell cycle progression and mitosis.[5]

The cell cycle entry of VSMCs is stimulated by a variety of growth factors produced from inflammatory cells, platelets, and the vascular cells where vascular injury occurs.[1] Although these growth factors, including platelet-derived growth factor (PDGF), basic fibroblast growth factor, insulin-like growth factor, and angiotensin II (Ang II), use distinct signaling pathways to promote DNA synthesis in VSMC, these signaling pathways must converge on common regulators of the cell cycle such as CDKs and CDKIs.[6] The final common pathway leading to G0/G1/S transition is the CDKs-induced hyperphosphorylation of the retinoblastoma gene product (Rb),[7] which functions as a molecular switch dedicating the cell to DNA replication. Hyperphosphorylation of Rb results in the release of the transcription factor E2F, which induces the expression of genes required for the progression through the S, G2, and M phases.[8] CDKIs such as $p21^{CIP}$ negatively regulate cell cycle progression by inhibiting cyclin/CDKs activity and phosphorylation of Rb, resulting in G1 arrest.[9] Progression of the cell cycle is therefore regulated by the balance between the levels and activities of cyclin-

Original received May 31, 2005; resubmission received August 9, 2005; revised resubmission received August 31, 2005; accepted August 31, 2005.

From the Department of Metabolic Medicine (M.I., H.M., K.T., K.K., T.M., T.K., T. Taguchi, K.N., M.Y., D.K., K.M., T. Toyonaga, T.N., E.A.), Faculty of Medical and Pharmaceutical Sciences, Kumamoto University, Kumamoto, and the Department of Physiological Chemistry and Metabolism (T.A.), Graduate School of Medicine, University of Tokyo, Japan.

*Both authors contributed equally to this work.

Correspondence to Hiroyuki Motoshima, Department of Metabolic Medicine, Faculty of Medical and Pharmaceutical Sciences, Kumamoto University, 1-1-1 Honjo, Kumamoto 860-8554, Japan. E-mail hmoto@gpo.kumamoto-u.ac.jp

Circulation Research is available at http://circres.ahajournals.org DOI: 10.1161/01.RES.0000185823.73556.06

CDK complexes, CDKIs, and other growth suppressor proteins such as p53.

Tumor suppressor p53 is tightly regulated by its phosphorylation state. Cellular stresses such as γ-irradiation induce Ser-15 phosphorylation of p53.[10,11] The phosphorylated p53 induces cell cycle arrest and/or apoptosis through the transcriptional regulation of p53 response genes such as $p21^{CIP}$.

Adenosine monophosphate-activated protein kinase (AMPK) plays a key role in the regulation of energy homeostasis and monitors cellular energy charge, acting as a "metabolic master switch" to regulate adenosine triphosphate concentrations in the face of stresses that reduce cellular energy levels.[12–14] AICAR (5-Aminoimidazole-4-carboxamide ribonucleoside) is a well-known activator of AMPK. AICAR is transported inside the cells through the adenosine transporter and phosphorylated by adenosine kinase[15] to form zeatin riboside-5-monophosphate (ZMP), which mimics the stimulatory action of AMP on AMPK.[16] Previous studies reported that AICAR could inhibit apoptosis in primary astrocytes[17] and endothelial cells.[18] On the other hand, AICAR has been reported to cause apoptosis in neuroblastoma cell lines[19] and B-cell chronic lymphocytic leukemia cells.[20]

Thus far, only 2 studies have reported the role of AMPK activation in VSMCs.[21,22] Whereas Rubin et al[21] reported the activation of AMPK with 2-deoxyglucose plus N_2, but not with AICAR, in rat carotid artery smooth muscle, Nagata et al[22] reported that AICAR activated AMPK in rat aortic SMCs and further inhibited Ang II-induced SMC proliferation. No information is available, however, on the effect of AICAR in human aortic SMCs (HASMCs). Therefore, in the present work, we determined whether AMPK activation by AICAR could suppress proliferation or induce apoptosis in HASMCs, and further investigated the mechanisms of AICAR-induced suppression of VSMC proliferation. We have found that AICAR exerts an antiproliferative effect through the activation of AMPK in HASMCs, and that the mechanism seems to involve cell cycle arrest through the upregulation of p53 and $p21^{CIP}$.

Materials and Methods

Cell Culture and Reagents

HASMCs were purchased from Clonetics (Walkersville, Md). For all experiments, early passaged (passages 4 to 7) SMCs were used. AICAR was obtained from Toronto Research Chemicals. We purchased 5′-amino-5′-deoxyadenosine (AMDA), dipyridamole, diethylmaleate (DEM), and PDGF-BB from Sigma.

Cell Proliferation Assay

We used 2 different methods, cell counting assay[23] and Alamar Blue assay[24] as described previously (see also expanded Materials and Methods available online at http://circres.ahajournals.org).

Determination of DNA Content Using Hoechst 33258 Dye

DNA content in SMCs was determined as an index for cell proliferation or for cytotoxity according to the instruction supplied by Thermo Labsystems (see also expanded Materials and Methods).

Experiments Using Adenoviral Vectors

An adenoviral vector expressing dominant negative (DN)-AMPK (Ad-DN-AMPK), which serves as a nonphosphorylatable T172A mutant of AMPK α-subunit[25] and contains a c-*myc* tag at the NH_2 terminus, was used to inhibit AMPK activity as described previously.[26] SMCs were infected with the indicated adenoviral vectors at 100 multiplicity of infection (100 MOI) for 2 hours. The medium was then changed to Dulbecco's modified eagle medium (DMEM) containing 0.2% fetal calf serum (FCS). After the incubation for 2 days, infected cells were stimulated with 10 ng/mL PDGF-BB or 15% FCS in the presence or absence of AICAR. In some experiments, cells were pretreated with AICAR for 4 hours. In experiments using inhibitors, inhibitors were added 30 minutes before AICAR treatment.

Cell Cycle Analysis

The fraction of cells present in each cell cycle phase (G0/G1, S, and G2/M) was determined by flow cytometry using a BD FACStar flow cytometer and ModiFit software from Verity House.

Detection of Apoptosis

A sandwich ELISA method was used to assess apoptosis using the Cell Death ELISA plus kit (Roche) as described previously.[27]

Western Blots

Western blotting was performed essentially as previously reported.[28]

Ex Vivo Experiments

Male Japanese white rabbits (Kyudo Co Ltd, Saga, Japan) were euthanized by overdose of Inactin. The descending thoracic aorta was rapidly excised and cleaned of connective tissues. The endothelium was removed by gently rubbing the vessel with wet cotton swab. The aorta was cut into 5-mm rings and the rings were cut open into strips. The aortic strips were stimulated without or with 15% FCS in the presence or absence of AICAR. After the stimulation, strips were homogenized in the lysis buffer. Western Blot analyses were performed as described above.

Experimental procedures for a real-time reverse transcription polymerase chain reaction (RT-PCR) analysis, a dual-luciferase assay for p53-dependent transcription, trypan blue exclusion assay, and detailed information for procedures described above are available in an expanded Materials and Methods section at http://circres.ahajournals.org.

Results

AICAR Suppresses Proliferation and DNA Synthesis of HASMCs Stimulated by PDGF-BB or 15% FCS

To determine the roles of AMPK on SMC proliferation, we first investigated the effect of AICAR on proliferation by the cell count assay. Treatment of HASMCs with PDGF-BB (10 ng/mL) or 15% FCS increased cell proliferation by ≈2.6-fold and ≈3.6-fold, respectively, compared with control cells incubated with 0.2% FCS. AICAR decreased the number of cells induced by PDGF-BB or 15% FCS in a dose-dependent manner (Figure 1A and 1B). Similar results were obtained in primary rabbit aortic SMCs (RASMCs) (supplemental Figure S1A and S1B).

We further investigated the inhibitory effect of AICAR on proliferation using Alamar Blue assay. Treatment with AICAR significantly reduced Alamar Blue fluorescence intensity in HASMCs stimulated with PDGF-BB or 15% FCS (Figure 1C). Microscopic observation after Alamar Blue assay confirmed that the decreased fluorescence intensity in AICAR-treated cells was due to the reduced cell number

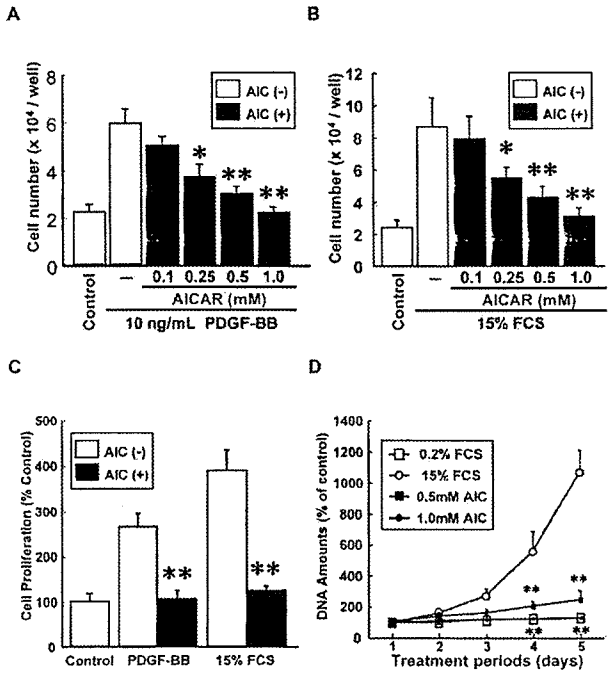

Figure 1. AICAR inhibits HASMC proliferation and DNA synthesis. A and B, Dose-dependent effect of AICAR on cell number of HASMCs stimulated by PDGF-BB (A) or FCS (B), respectively. Quiescent cells on 6-well dish were stimulated with PDGF-BB (10 ng/mL) or FCS (15%) in the presence (solid bars) or absence (open bars) of indicated concentrations of AICAR for 4 days. Cell number was determined by the cell counting. C, Effect of AICAR on Alamar Blue reduction. Quiescent HASMCs on 96-well plate were treated as described above. After 4 days, culture medium was replaced with DMEM containing 10% Alamar Blue. Cell proliferation was determined by measuring fluorescence intensity. Cell proliferation is expressed as a percentage of that in the nonstimulated condition (control). D, Effect of AICAR on DNA synthesis. Quiescent HASMCs on 96-well plate were treated as described above and harvested at the indicated time points. Total cellular DNA content was determined by measuring fluorescence intensity. DNA content is expressed as a percentage of that harvested at day 0 (just before mitotic stimulation). Data are shown as mean±SEM from at least 3 separate experiments. $^{*}P<0.05$, $^{**}P<0.01$ as compared with PDGF or 15% FCS alone.

(data not shown). Furthermore, treatment with 15% FCS increased DNA synthesis in HASMCs, and AICAR significantly suppressed the increase in DNA synthesis in a dose-dependent manner (Figure 1D). Notably, AICAR treatment did not reduce DNA amounts in cells compared with the control cells treated with 0.2% FCS, suggesting the inhibitory effect of AICAR on DNA synthesis rather than the loss of cellular DNA due to a cytotoxic effect.

AICAR Activates AMPK in HASMCs, RASMCs, and Isolated Aortic Strips

Next, we investigated the effect of AICAR on the phosphorylation of AMPK in HASMCs and RASMCs by Western blot analyses using an antibody specific for the Thr-172 phosphorylation of α-subunit of AMPK (α-AMPK). Treatment with AICAR for 2 hours markedly increased the phosphorylation of α-AMPK compared with the vehicle-treated control in HASMCs and RASMCs (Figure 2A and 2B). Although the

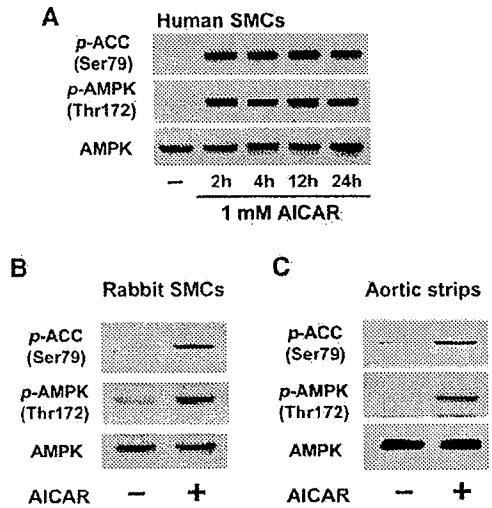

Figure 2. Effect of AICAR on the phosphorylation of AMPK and ACC. A and B, Quiescent HASMCs (A) or RASMCs (B) were treated without or with 1 mmol/L AICAR for indicated periods (A) or for 2 hours (B). C, Endothelium-denuded rabbit aortic strips were treated without or with 1 mmol/L AICAR for 4 hours. Western blot analyses were performed using 30 μg of protein in each lane. AMPK phosphorylation (*p*-AMPK) and ACC phosphorylation (*p*-ACC) was assessed. Total AMPK was detected with anti-pan-α-AMPK antibody. Representative blots of 3 independent experiments are shown.

increased Thr-172 phosphorylation of α-AMPK is indicative of the activation of this kinase, we also immunoblotted with anti-phospho-ACC (Ser-79) antibody to ascertain whether increased phosphorylation of AMPK had effects on downstream target proteins. In accordance with AMPK activation, phosphorylation of ACC was markedly elevated in AICAR-treated HASMCs and RASMCs (Figure 2A and 2B). We investigated the time course of AICAR effect on phosphorylation of AMPK and ACC. Phosphorylation of these molecules by AICAR was sustained over 24 hours in HASMCs (Figure 2A).

Further, we investigated whether AICAR could activate AMPK in isolated aortic strips. Endothelium-denuded aortic strips were stimulated with 1 mmol/L AICAR for 2 hours. Increased phosphorylation of AMPK and ACC were observed in AICAR-treated strips (Figure 2C). These results demonstrate that AICAR activates AMPK and regulates downstream enzyme ACC in primary cultured SMCs (in vitro) and in isolated aortic strips (ex vivo).

Inhibition of AMPK Activity by Inhibitors of AICAR Function or DN-AMPK Blocks the Growth-Suppressive Effect of AICAR

To exclude the possibility that the inhibitory effect of AICAR on SMC proliferation was caused by mechanisms other than AMPK activation, we investigated the effects of 2 different inhibitors of AICAR function, dipyridamole and AMDA. Dipyridamole inhibits transport of AICAR into cells by inhibiting an adenosine transporter, and AMDA inhibits the phosphorylation of AICAR by blocking the adenosine kinase in the cells.[19,29,30] Pretreatment with dipyridamole completely blocked the inhibitory effect of AICAR on proliferation

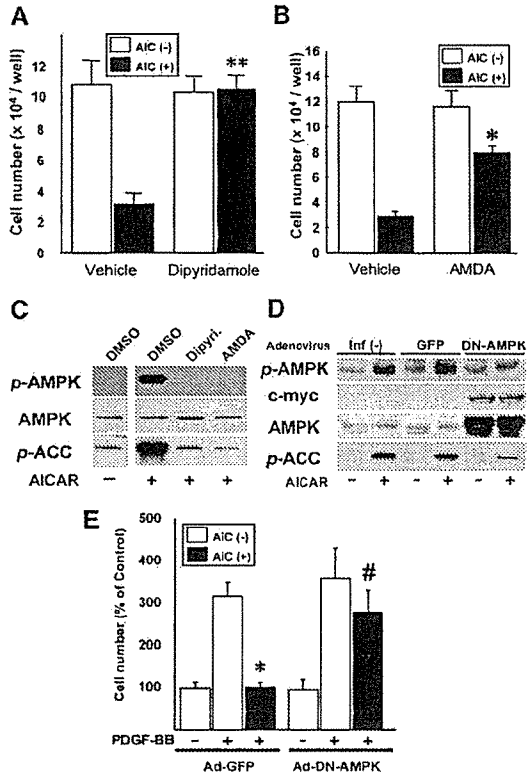

Figure 3. Effects of the inhibition of AMPK activity by inhibitors of AICAR function or by DN-AMPK on the antiproliferative effect of AICAR. A and B, Quiescent HASMCs were pretreated with dipyridamole (10 μmol/L; A), AMDA (10 μmol/L; B), or vehicle (DMSO) for 30 minutes. Cells were then incubated for 4 days without (open bars) or with (solid bars) 1 mmol/L AICAR in the presence of 15% FCS and inhibitors. Cell counting assay was performed. Data are mean±SEM (n=6) from 3 independent experiments. The significance versus AICAR-treated cells with vehicle was expressed as $^*P<0.01$. C, Quiescent HASMCs were pretreated with inhibitors or vehicle (DMSO) for 30 minutes and then stimulated without or with 1 mmol/L AICAR for 2 hours. D, Quiescent HASMCs without infection [Inf (-)] or infected with the indicated adenoviral vector were treated without or with 1 mmol/L AICAR for 2 hours. Western blot analyses were performed. Representative blots of 3 independent experiments are shown. E, Quiescent HASMCs infected with the indicated adenoviral vector were incubated for 4 days without (open bars) or with (solid bars) 1 mmol/L AICAR in the presence of 15% FCS. Cell counting assay was performed. $^*P<0.01$ as compared with 15% FCS alone in Ad-GFP-infected cells; $\#P<0.01$ as compared with AICAR-treated Ad-GFP-infected cells.

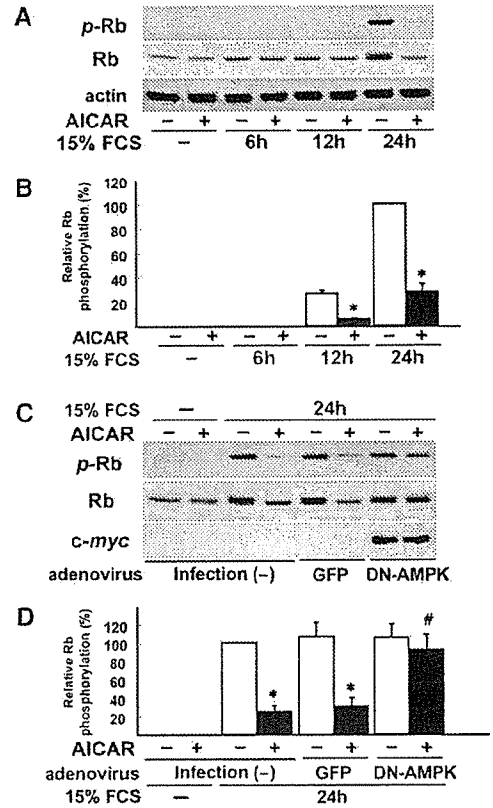

Figure 4. Effect of AICAR on Rb phosphorylation in HASMCs. A and B, Quiescent HASMCs were pretreated without or with 1 mmol/L AICAR in DMEM containing 0.2% FCS for 4 hours. Then cells were stimulated without or with 15% FCS for the indicated periods. C and D, HASMCs were not infected [Infection (-)prsqb] or infected with Ad-GFP or Ad-DN-AMPK and were made quiescent. Cells were then treated without or with 1 mmol/L AICAR for 4 hours and stimulated with 15% FCS for 24 hours. Western blot analyses were performed to detect total (Rb), phosphorylated Rb (*p*-Rb), and actin to confirm equal loading. The expression of DN-AMPK was confirmed by blotting with anti-c-*myc* antibody. Representative blots (A and C) and relative levels of Rb phosphorylation (B and D) are shown. The data are quantified from 3 independent experiments. $^*P<0.01$ as compared with 15% FCS alone; $\#P<0.01$ as compared with AICAR-treated Ad-GFP-infected cells.

(Figure 3A). AMDA partially but significantly blocked the inhibitory effect of AICAR on proliferation (Figure 3B). Pretreatment with these inhibitors completely inhibited AICAR-induced phosphorylation of AMPK and ACC (Figure 3C). These results indicated that ZMP formation through both transport and phosphorylation of AICAR is required for the suppression of growth by AICAR, suggesting that AMPK activation is a key process for an inhibitory effect of AICAR on SMC proliferation.

To further confirm the involvement of AMPK on growth-suppressive effect of AICAR, we performed the experiments using an adenoviral vector expressing DN-AMPK, which has been reported to inhibit AMPK activation as a nonphosphorylatable T172A mutant.[25–26] Overexpression of DN-AMPK, but not of green fluorescent protein (GFP) (control), suppressed AICAR-induced phosphorylation of AMPK and ACC (Figure 3D). Overexpression of DN-AMPK was confirmed by Western blotting using both anti-c-*myc* and anti-pan-α-AMPK antibodies. In HASMCs infected with Ad-GFP, AICAR completely suppressed proliferation (Figure 3E) as observed in Figure 1A. DN-AMPK significantly inhibited the suppressive effect of AICAR on proliferation. These results indicate the involvement of AMPK on AICAR-induced suppression of SMC proliferation.

AICAR Inhibits Phosphorylation of Rb

Next, we examined the effect of AICAR on the phosphorylation of Rb stimulated with 15% FCS or PDGF, as phosphorylation of Rb has been reported to be a critical and common event during cell proliferation process.[7–9,31] Increased phosphorylation of Rb was detected 12 hours after stimulation with FCS. Rb phosphorylation was further in-

creased in a time-dependent manner, indicating the cell cycle progression induced by FCS. AICAR significantly inhibited FCS-induced Rb phosphorylation (Figure 4A and 4B). AICAR also strongly suppressed PDGF-induced Rb phosphorylation (supplemental Figure S2A). These results suggest that AICAR suppresses a G1 event in cell cycle progression. This suppressive effect of AICAR on Rb phosphorylation was inhibited by overexpression of DN-AMPK but not by that of the control GFP (Figure 4C and 4D and supplemental Figure S2B).

AMPK Induces G1 Cell Cycle Arrest but Not Apoptosis

Reduction in cell number induced by AMPK activation could be the result of the inhibition of proliferation or increased cell death. To distinguish these possibilities, we first investigated the effect of AMPK on cell cycle progression using a flow cytometry analysis. Compared with control cells treated with 15% FCS, AICAR significantly increased the cells in the G0/G1 phase (from 76.0±2.2% to 88.6±1.9%) and decreased those in S (from 14.6±0.8% to 5.7±1.4%) and G2/M phase (from 9.4±1.5% to 5.7±1.5%) (Figure 5A). This effect of AICAR was statistically significant ($P<0.01$, n=5) and was almost completely inhibited either by coincubation with dipyridamole or by overexpression of DN-AMPK (supplemental Figure S3). These data suggest AMPK activation causes G1 arrest in HASMCs.

To examine the second possibility, we investigated whether AICAR could induce cell death. In trypan blue exclusion assay, DEM significantly decreased viable cell number. In contrast, no difference was observed in the rate of appearance for dead cells between AICAR-treated and vehicle-treated HASMCs (Figure 5B). Using a cell death ELISA quantitative assay, no differences were observed in the rates of cytoplasmic DNA-histone complex formation between HASMCs treated with AICAR and those with 15% FCS alone (Figure 5C). In addition, increased population in sub-G1 was not observed even after 72 hours in AICAR-treated HASMCs (data not shown). These data indicate that AMPK-induced cell number reduction in HASMCs is due to the inhibition of cell proliferation rather than cell death.

AMPK Increases the Expression of $p21^{CIP}$

We further investigated the effect of AMPK on the protein expression of CDKIs $p21^{CIP}$ and $p27^{KIP}$. Increased expression of $p21^{CIP}$ protein but not of $p27^{KIP}$ was observed in AICAR-treated HASMCs compared with those treated with 15% FCS alone from 6 hours to 24 hours after stimulation with FCS (Figure 6A and 6B). FCS stimulation decreased $p27^{KIP}$ expression. AICAR did not block the FCS-induced reduction of $p27^{KIP}$ (Figure 6A, middle panel). Expression of $p21^{CIP}$ has been reported to be regulated both in p53-dependent and -independent manners. To test whether AMPK increases the $p21^{CIP}$ expression through the activation of p53, we examined the effect of AICAR on expression and Ser-15 phosphorylation of p53. AICAR increased phosphorylated p53 and its protein expression, and also increased the expression of $p21^{CIP}$ (Figure 6C) in a dose-dependent manner. The increase in p53 protein was associated with an increased $p21^{CIP}$ level.

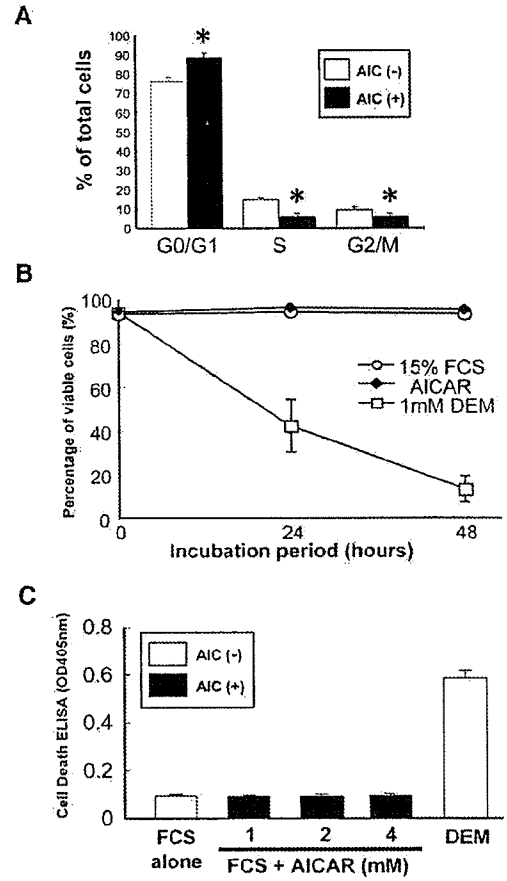

Figure 5. Effect of AICAR on cell cycle progression, viability, and apoptosis. A, Cell cycle distribution in AICAR-treated HASMCs. Data are expressed as a percentage of total cells. Each value represents mean±SEM from 5 independent experiments. *$P<0.01$ as compared with 15% FCS alone (open bars). B, Viability of HASMCs treated with AICAR. HASMCs were treated without (open circles) or with (closed squares) 1 mmol/L AICAR in DMEM containing 15% FCS. As a positive cytotoxic control, treatment with 1 mmol/L DEM was performed in DMEM containing 15% FCS. After the indicated period, viability was determined by trypan blue exclusion assay. Results are expressed as a percentage of viable cells to total cells counted. C, AICAR does not induce apoptosis in HASMCs. HASMCs were treated without (open bars) or with (solid bars) indicated concentrations of AICAR or 1 mmol/L DEM in DMEM containing 15% FCS for 24 hours. Apoptosis was assessed using the cell death ELISA and expressed as OD at 405 nm. Results (mean±SEM) were from 3 independent experiments.

We further investigated the effect of AICAR on the mRNA expression of $p21^{CIP}$ and p53 using a real-time RT-PCR analysis. AICAR increased the expression of $p21^{CIP}$ mRNA, whereas no significant change was observed in the mRNA expression of p53 (supplemental Figure S4A), indicating the transcriptional and post-transcriptional mechanisms for $p21^{CIP}$ and p53 upregulation, respectively. We further investigated whether p53 is functionally activated in HASMCs treated with AICAR using a reporter assay system. This dual-luciferase assay revealed that p53-dependent transcription in AICAR-treated cells significantly increased compared with both control cells and those treated with 15% FCS alone (supplemental Figure S4B).

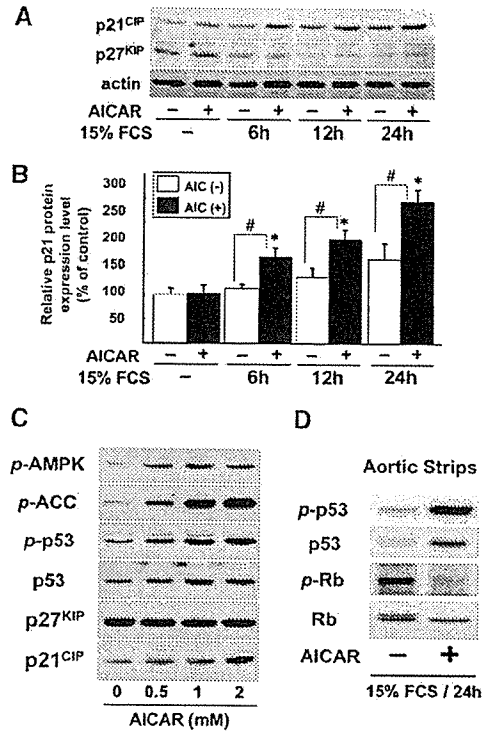

Figure 6. Effect of AICAR on the expression of p21, p27, and p53. A and B, Quiescent HASMCs were treated without (open bars) or with (solid bars) 1 mmol/L AICAR for the indicated periods in DMEM containing 15% FCS. Controls without FCS stimulation were harvested just before adding FCS (lane 1) or just after adding AICAR alone (lane 2). Representative blots (A) for $p21^{CIP}$ and $p27^{KIP}$ protein from 3 independent experiments and quantitative data for $p21^{CIP}$ protein (B) are shown. Actin was detected to confirm equal loading. *$P<0.05$ as compared with control incubated without 15% FCS nor AICAR; #$P<0.05$ as compared with 15% FCS alone at each time point. C, Quiescent HASMCs were treated without or with the indicated concentrations of AICAR in DMEM without FCS for 3 hours. D, Endothelium-denuded aortic strips were treated without or with 1 mmol/L AICAR for 4 hours, and then FCS was added at the final concentration of 15%. After 24 hours, strips were harvested. Representative blots of 3 independent experiments are shown.

Finally, we investigated whether AMPK activation could exhibit several effects in isolated rabbit aortas, as observed in cultured SMCs. As observed in Figure 2C, AICAR significantly increased the phosphorylation of AMPK and ACC in our ex vivo experimental system. Furthermore, increased p53 phosphorylation and p53 protein expression were accompanied with the decreased Rb phosphorylation in AICAR-treated aortic strips (Figure 6D). The increased levels of phosphorylated p53 and p53 protein were dependent on the activation of AMPK, as either dipyridamole or AMDA completely blocked these AICAR-induced changes in p53 (supplemental Figure S4C). These findings indicate that AMPK exhibits the growth-inhibitory effect in aortic SMCs in vivo, as observed in cultured SMCs and in aortic strips.

Discussion

In the present study, we have demonstrated for the first time that AMPK inhibited FCS- and PDGF-induced proliferation in human aortic SMCs. Similar results were also obtained in rabbit aortic SMCs. The mechanism of growth suppression induced by AMPK turned out to be a cell cycle arrest at G1 phase but not by an apoptosis. We further investigated how AMPK induces cell cycle arrest in SMCs, and found that activation of AMPK increased the CDKI $p21^{CIP}$ protein through the upregulation of p53, which in turn inhibited the Rb phosphorylation required for cell cycle progression.

Transport of AICAR into cells has been studied previously.[20,29,32] Lopez et al reported that adenosine inhibited the accumulation of ZMP in AICAR-treated Jurkat cells via competition with AICAR transport into the cells.[32] Dipyridamole and AMDA were reported to block adenosine-induced apoptosis by inhibiting AMPK activation.[29] Further, adenosine and 5-iodotubercidine, another adenosine kinase inhibitor, were reported to inhibit apoptosis and AMPK phosphorylation in B-cell chronic lymphocytic leukemia cells treated with AICAR.[20] Because of these reports, we investigated the effect of dipyridamole and AMDA on AICAR-induced growth suppression. As expected, both inhibitors blocked the inhibitory effect of AICAR on SMC proliferation, as well as AICAR-induced phosphorylation of AMPK and ACC. These observations indicate that both uptake and phosphorylation of AICAR are necessary for the activation of AMPK by AICAR and AICAR-induced suppression of SMC proliferation, suggesting that AMPK activation is required for the growth suppression of AICAR. Adenosine was reported to induce apoptosis in HASMCs via A2b adenosine receptor and cAMP-dependent pathways.[33] Although AICAR is an adenosine analogue, treatment of HASMCs with adenosine or AICAR seems to induce totally different cellular events, apoptosis or growth-suppression without apoptosis, respectively. We also demonstrated that DN-AMPK inhibited the growth suppression by AICAR, which further supports the involvement of AMPK in AICAR-induced suppression of SMC proliferation.

Recently, Nagata et al reported that AICAR-induced AMPK activation inhibited Ang II-induced proliferation of VSMCs derived from rat aortas.[22] Their observations are consistent with our present study, although the mitotic stimulations used were different. To confirm their observations, we performed several preliminary experiments. Indeed, AICAR inhibited proliferation induced by Ang II in HASMCs, and we also found that AICAR induced cell cycle arrest in Ang II-treated HASMCs (unpublished data, 2004). These findings indicate activation of AMPK by AICAR induces cell cycle arrest and suppresses proliferation in SMCs treated with either PDGF-BB, Ang II, or FCS.

As mentioned above, AICAR has been reported to be able to either induce or inhibit apoptosis depending on the cell types.[17–20] In HASMCs, AICAR did not induce apoptosis. AICAR may have an anti-apoptotic effect in HASMCs, as AICAR treatment significantly reduced sub-G1 fraction in SMCs growing without rendering quiescent (10.6±2.2% of control cells or 4.7±0.9% of those treated with AICAR were located in sub-G1 fraction, respectively; $P<0.01$, n=5 each; unpublished data, 2004). Further intensive investigations are required to elucidate for the anti-apoptotic effect of AICAR in SMCs.

In the present study, AICAR increased p53 and p21 protein expression, as well as Ser-15 phosphorylated p53, in HASMCs and isolated rabbit aortas. Our results are consistent with a report by Imamura et al.[34] They reported that AICAR suppressed proliferation via p53 phosphorylation and its accumulation in HepG2 cells. It has also been reported that Ser-15 modification of p53 results in decreased binding affinity between mdm2 and p53, thereby suppressing the degradation of p53 protein, resulting in p53 accumulation.[35] In response to stresses such as hypoxia or DNA damage, p53 is activated by several mechanisms, including the phosphorylation, and the activated p53 induces either cell cycle arrest or apoptosis.[36] In our present study, activation of p53 signaling in HASMCs by AICAR was confirmed using both reporter-gene analysis and RT-PCR analysis for $p21^{CIP}$.

It has been reported that adenovirus-mediated overexpression of p21 or p53 inhibits vascular SMC proliferation and suppresses neointima formation in the rat carotid artery,[37,38] suggesting that p21 or p53 functions to suppress SMC proliferation and neointima formation.

The most striking effect of AICAR was the induction of a CDKI $p21^{CIP}$. Inactivation of CDKs by CDKIs maintains Rb at hypophosphorylated state, which keeps E2F inactive.[39] E2F is required for induction of several factors essential for S phase progression; thus, maintaining E2F in an inactive state leads to G1 arrest. In our present study, upregulation of $p21^{CIP}$ and decline in Rb phosphorylation by AICAR were observed, indicating that $p21^{CIP}$ plays a major role in AICAR-induced G1 arrest in HASMCs.

In the present study, we have demonstrated that AICAR treatment increased Ser-15 phosphorylation and protein expression of p53 in HASMCs and isolated rabbit aortas. Because either dipyridamole or overexpression of DN-AMPK completely blocked these events, it is suggested that either AMPK itself or downstream kinase is involved in AICAR-induced p53 upregulation. Although we have not tested whether Ser-15 phosphorylation of p53 is necessary for the AICAR-induced cell cycle arrest, during the preparation of this article, Jones et al[40] reported that activation of AMPK either by glucose limitation, treatment with AICAR, or overexpression of constitutive active AMPK induced a G1 cell cycle arrest via AMPK-dependent Ser-15 phosphorylation of p53 in primary mouse embryonic fibroblasts. In addition, they demonstrated that Ser-15 phosphorylation of p53 was required for AMPK-induced cell cycle arrest using mouse embryonic fibroblasts derived from $p53^{Ser18Ala}$ mice, in which Ser-18 of mouse p53 corresponding to Ser-15 of human p53 was mutated. Therefore, we speculated that AICAR phosphorylated p53 protein and subsequently increased the amount of both p53 protein and phosphorylated p53 protein because the phosphorylation of p53 protein has been reported to increase the stability of this protein.[35,36]

The Ser-15 phosphorylation of p53 has been reported to be mediated by 3 distinct protein kinases, Ataxia-Telangiectasia Mutated (ATM), ATM and Rad3-related (ATR), and DNA-dependent protein kinase (DNA-PK) in response to DNA damage.[10–11,41] Jones et al[40] demonstrated that AICAR-induced Ser-15 phosphorylation of p53 was ATM-independent but AMPK-dependent, suggesting the possibility that AMPK may directly phosphorylate Ser-15 of p53. In our present study, it was not tested whether AMPK activation by AICAR could activate ATM, ATR, or DNA-PK and whether these kinases could phosphorylate p53 under our experimental conditions. Further investigation is required to understand the mechanisms of AICAR-induced p53 phosphorylation and accumulation in HASMCs.

In conclusion, this is the first study to show that activation of AMPK by AICAR effectively suppressed cell cycle progression in primary human VSMCs and isolated rabbit aortas, suggesting that AMPK could be a target for the prevention of vascular proliferative disorders such as atherosclerosis.

Acknowledgments

This work was supported by a Grant-in-Aid for Scientific Research from Japan Society for the Promotion of Science, Japan (No. 16046219 to E.A. and No. 16590889 to T.N.). We thank Dr Kenshi Ichinose in our laboratory and Dr Miku Kato, as well as members in Kumamoto University School of Medicine Core Laboratory for Medical Research and Education for helpful advice and assistance.

References

1. Ross R. The pathogenesis of atherosclerosis: a perspective for the 1990s. *Nature.* 1993;362:801–809.
2. Sherr CJ. Cancer cell cycles. *Science.* 1996;274:1672–1677.
3. Sherr CJ. Mammalian G1 cyclins. *Cell.* 1993;73:1059–1065.
4. Hunter T. Braking the cycle. *Cell.* 1993;75:839–841.
5. Morgan DO. Principles of CDK regulation. *Nature.* 1995;374:131–134.
6. Lukas J, Bartkova J, Bartek J. Convergence of mitogenic signalling cascades from diverse classes of receptors at the cyclin D-cyclin-dependent kinase-pRb-controlled G1 checkpoint. *Mol Cell Biol.* 1996;16:6917–6925.
7. Nevins JR, Leone G, DeGregori J, Jakoi L. Role of the Rb/E2F pathway in cell growth control. *J Cell Physiol.* 1997;173:233–236.
8. Weinberg RA. The retinoblastoma protein and cell cycle control. *Cell.* 1995;81:323–330.
9. Hunter T, Pines J. Cyclins and cancer: II: cyclin D and CDK inhibitors come of age. *Cell.* 1994;79:573–582.
10. Shieh SY, Ikeda M, Taya Y, Prives C. DNA damage-induced phosphorylation of p53 alleviates inhibition by MDM2. *Cell.* 1997;91:325–334.
11. Canman CE, Lim DS, Cimprich KA, Taya Y, Tamai K, Sakaguchi K, Appella E, Kastan MB, Siliciano JD. Activation of the ATM kinase by ionizing radiation and phosphorylation of p53. *Science.* 1998;281:1677–1679.
12. Hardie DG. Minireview: the AMP-activated protein kinase cascade: the key sensor of cellular energy status. *Endocrinology.* 2003;144:5179–5183.
13. Carling D. The AMP-activated protein kinase cascade: a unifying system for energy control. *Trends Biochem Sci.* 2004;29:18–24.
14. Kahn BB, Alquier T, Carling D, Hardie DG. AMP-activated protein kinase: ancient energy gauge provides clues to modern understanding of metabolism. *Cell Metab.* 2005;1:15–25.
15. Young ME, Radda GK, Leighton B. Activation of glycogen phosphorylase and glycogenolysis in rat skeletal muscle by AICAR, an activator of AMP-activated protein kinase. *FEBS Lett.* 1996;382:43–47.
16. Merrill GF, Kurth EJ, Hardie DG, Winder WW. AICA riboside increases AMP-activated protein kinase, fatty acid oxidation, and glucose uptake in rat muscle. *Am J Physiol.* 1997;273:E1107–E1112.
17. Blazquez C, Geelen MJ, Velasco G, Guzman M. The AMP-activated protein kinase prevents ceramide synthesis de novo and apoptosis in astrocytes. *FEBS Lett.* 2001;489:149–153.
18. Ido Y, Carling D, Ruderman N. Hyperglycemia-induced apoptosis in human umbilical vein endothelial cells: inhibition by the AMP-activated protein kinase activation. *Diabetes.* 2002;51:159–167.
19. Garcia-Gil M, Pesi R, Perna S, Allegrini S, Giannecchini M, Camici M, Tozzi MG. 5′-aminoimidazole-4-carboxamide riboside induces apoptosis in human neuroblastoma cells. *Neuroscience.* 2003;117:811–820.
20. Campas C, Lopez JM, Santidrian AF, Barragan M, Bellosillo B, Colomer D, Gil J. Acadesine activates AMPK and induces apoptosis in B-cell

chronic lymphocytic leukemia cells but not in T lymphocytes. *Blood.* 2003;101:3674–3680.
21. Rubin LJ, Magliola L, Feng X, Jones AW, Hale CC. Metabolic activation of AMP kinase in vascular smooth muscle. *J Appl Physiol.* 2005;98: 296–306.
22. Nagata D, Takeda R, Sata M, Satonaka H, Suzuki E, Nagano T, Hirata Y. AMP-activated protein kinase inhibits angiotensin II-stimulated vascular smooth muscle proliferation. *Circulation.* 2004;110:444–451.
23. Yu SM, Tsai SY, Guh JH, Ko FN, Teng CM, Ou JT. Mechanism of catecholamine-induced proliferation of vascular smooth muscle cells. *Circulation.* 1996;94:547–554.
24. Hattori Y, Suzuki M, Hattori S, Kasai K. Vascular smooth muscle cell activation by glycated albumin (Amadori adducts). *Hypertension.* 2002; 39:22–28.
25. Ouchi N, Kobayashi H, Kihara S, Kumada M, Sato K, Inoue T, Funahashi T, Walsh K. Adiponectin stimulates angiogenesis by promoting cross-talk between AMP-activated protein kinase and Akt signaling in endothelial cells. *J Biol Chem.* 2004;279:1304–1309.
26. Sakoda H, Ogihara T, Anai M, Fujishiro M, Ono H, Onishi Y, Katagiri H, Abe M, Fukushima Y, Shojima N, Inukai K, Kikuchi M, Oka Y, Asano T. Activation of AMPK is essential for AICAR-induced glucose uptake by skeletal muscle but not adipocytes. *Am J Physiol Endocrinol Metab.* 2002;282:E1239–E1244.
27. Geng YJ, Wu Q, Muszynski M, Hansson GK, Libby P. Apoptosis of vascular smooth muscle cells induced by in vitro stimulation with interferon-gamma, tumor necrosis factor-alpha, and interleukin-1 beta. *Arterioscler Thromb Vasc Biol.* 1996;16:19–27.
28. Motoshima H, Wu X, Mahadev K, Goldstein BJ. Adiponectin suppresses proliferation and superoxide generation and enhances eNOS activity in endothelial cells treated with oxidized LDL. *Biochem Biophys Res Commun.* 2004;315:264–271.
29. Saitoh M, Nagai K, Nakagawa K, Yamamura T, Yamamoto S, Nishizaki T. Adenosine induces apoptosis in the human gastric cancer cells via an intrinsic pathway relevant to activation of AMP-activated protein kinase. *Biochem Pharmacol.* 2004;67:2005–2011.
30. Nakamaru K, Matsumoto K, Taguchi T, Suefuji M, Murata Y, Igata M, Kawashima J, Kondo T, Motoshima H, Tsuruzoe K, Miyamura N, Toyonaga T, Araki E. AICAR, an activator of AMP-activated protein kinase, down-regulates the insulin receptor expression in HepG2 cells. *Biochem Biophys Res Commun.* 2005;328:449–454.
31. Peeper DS, Upton TM, Ladha MH, Neuman E, Zalvide J, Bernards R, DeCaprio JA, Ewen ME. Ras signalling linked to the cell-cycle machinery by the retinoblastoma protein. *Nature.* 1997;386:177–181.
32. Lopez JM, Santidrian AF, Campas C, Gil J. 5-Aminoimidazole-4-carboxamide riboside induces apoptosis in Jurkat cells, but the AMP-activated protein kinase is not involved. *Biochem J.* 2003;370:1027–1032.
33. Peyot ML, Gadeau AP, Dandre F, Belloc I, Dupuch F, Desgranges C. Extracellular adenosine induces apoptosis of human arterial smooth muscle cells via A(2b)-purinoceptor. *Circ Res.* 2000;86:76–85.
34. Imamura K, Ogura T, Kishimoto A, Kaminishi M, Esumi H. Cell cycle regulation via p53 phosphorylation by a 5′-AMP activated protein kinase activator, 5-aminoimidazole- 4-carboxamide-1-beta-D-ribofuranoside, in a human hepatocellular carcinoma cell line. *Biochem Biophys Res Commun.* 2001;287:562–567.
35. Giaccia AJ, Kastan MB. The complexity of p53 modulation: emerging patterns from divergent signals. *Genes Dev.* 1998;12:2973–2983.
36. Evan G, Littlewood T. A matter of life and cell death. *Science.* 1998; 281:1317–1322.
37. Condorelli G, Aycock JK, Frati G, Napoli C. Mutated p21/WAF/CIP transgene overexpression reduces smooth muscle cell proliferation, macrophage deposition, oxidation-sensitive mechanisms, and restenosis in hypercholesterolemic apolipoprotein E knockout mice. *FASEB J.* 2001; 15:2162–2170.
38. Yonemitsu Y, Kaneda Y, Tanaka S, Nakashima Y, Komori K, Sugimachi K, Sueishi K. Transfer of wild-type p53 gene effectively inhibits vascular smooth muscle cell proliferation in vitro and in vivo. *Circ Res.* 1998;82: 147–156.
39. Toyoshima H, Hunter T. p27, a novel inhibitor of G1 cyclin-Cdk protein kinase activity, is related to p21. *Cell.* 1994;78:67–74.
40. Jones RG, Plas DR, Kubek S, Buzzai M, Mu J, Xu Y, Birnbaum MJ, Thompson CB. AMP-activated protein kinase induces a p53-dependent metabolic checkpoint. *Molecular Cell.* 2005;18:283–293.
41. Banin S, Moyal L, Shieh S, Taya Y, Anderson CW, Chessa L, Smorodinsky NI, Prives C, Reiss Y, Shiloh Y, Ziv Y. Enhanced phosphorylation of p53 by ATM in response to DNA damage. *Science.* 1998;281: 1674–1677.

Available online at www.sciencedirect.com
SCIENCE DIRECT
ELSEVIER
Biochemical and Biophysical Research Communications 341 (2006) 703–707
BBRC
www.elsevier.com/locate/ybbrc

A negative feedback system between brain serotonin systems and plasma active ghrelin levels in mice

Katsunori Nonogaki *, Kana Ohashi-Nozue, Yoshitomo Oka

Center of Excellence, Division of Molecular Metabolism and Diabetes, Tohoku University Graduate School of Medicine, Japan

Received 4 January 2006
Available online 18 January 2006

Abstract

Brain serotonin (5-hydroxytryptamine; 5-HT) systems contribute to regulate eating behavior and energy homeostasis. 5-HT2C receptors and 5-HT1B receptors have been shown to mediate anorexic effects of 5-HT drugs such as D-fenfluramine, which stimulates 5-HT release and inhibits 5-HT reuptake, and *m*-chlorophenylpiperazine (mCPP), a 5-HT2C receptor agonist. Here, we report that 24-h fasting increased the expression of hypothalamic 5-HT2C receptor and 5-HT1B receptor genes in association with increases in plasma active ghrelin levels compared with fed state in mice. Treatment with mCPP or fenfluramine significantly inhibited the increases in plasma active ghrelin levels. mCPP or fenfluramine significantly increased the expression of hypothalamic pro-opiomelanocortin and cocaine- and amphetamine-regulated transcript genes while having no significant effects on the expression of hypothalamic neuropeptide Y, agouti-related protein, and ghrelin genes. These results suggest that there is a negative feedback system between brain 5-HT systems and plasma active ghrelin levels in energy homeostasis in mice.

Keywords: Serotonin; 5-HT2C receptor; 5-HT1B receptor; Ghrelin; Neuropeptide; POMC; CART; AGRP; Hypothalamus; Eating behavior; Energy homeostasis; Gene expression; mCPP; Fenfluramine

Mice with a mutated serotonin (5-hydroxytryptamine; 5-HT) 5-HT2C receptor gene display leptin-independent hyperphagia and hyperactivity that leads to a late onset of obesity associated with the secondary leptin resistance [1–3]. Several lines of evidence indicate that 5-HT2C receptors contribute to mediate the anorexic actions of 5-HT agonists such as *m*-chlorophenylpiperazine (mCPP) and 5-HT reuptake inhibitors such as D-fenfluramine and D-norfenfluramine [1,4,5]. These finding indicate that brain 5-HT systems via 5-HT2C receptors contribute to the regulation of eating behavior and energy homeostasis. In addition, 5-HT1B receptors have been suggested to mediate the anorexic actions of mCPP and D-fenfluramine in mice [6]. Activation of 5-HT2C receptor and 5-HT1B receptor signaling might therefore coordinate to suppress food intake.

The link between brain 5-HT systems and neuropeptides or gut peptides in the regulation of feeding and energy homeostasis, however, is still unclear. Ghrelin is an orexigenic peptide, secreted by stomach [7–9]. Fasting elevates plasma ghrelin levels, while feeding reduces the levels in animals and humans [8–10]. There are two forms of ghrelin, an active ghrelin with bioactivity and des-acyl ghrelin without biologic activity [10–12]. Because only the acylated form of ghrelin is active, measuring the acylated form of ghrelin might be advantageous.

In the present study, to determine the relationship between brain 5-HT systems and plasma ghrelin levels in the regulation of energy homeostasis, we investigated: (1) alterations of the expression of hypothalamic 5-HT2C and 5-HT1B receptor genes induced by fasting and feeding, (2) the effects of mCPP or fenfluramine on plasma active ghrelin levels, and (3) the effects of mCPP or fenfluramine on the gene expression of hypothalamic neuropeptides that

* Corresponding author. Fax: +81 22 717 7612.
E-mail address: knonogaki-tky@umin.ac.jp (K. Nonogaki).

0006-291X/$ - see front matter © 2006 Elsevier Inc. All rights reserved.
doi:10.1016/j.bbrc.2006.01.021